Merentutkimuslaitos
Havsforskninginstitutet
Finnish Institute of
Marine Research

A THEORETICAL AND EXPERIMENTAL STUDY
OF THE SELF-SIMILARITY CONCEPT

Rein Tamsalu and Kai Myrberg

A ONE-DIMENSIONAL THERMODYNAMIC AIR-ICE-WATER MODEL:
TECHNICAL AND ALGORITHM DESCRIPTION REPORT

Bin Cheng and Jouko Launiainen

LITERATURE REVIEW ON MICROBIOLOGY OF AGGREGATES
ORIGINATING FROM PHYTOPLANKTON BLOOMS

Susanna Hietanen

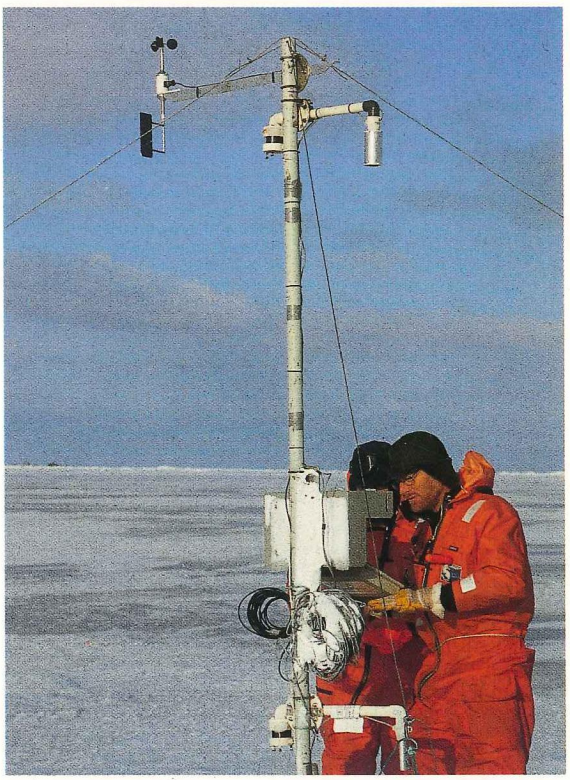

No. 37
1998

MERI

Report Series of the Finnish
Institute of Marine Research

MERI – Report Series of the Finnish Institute of Marine Research No. 37, 1998

A THEORETICAL AND EXPERIMENTAL STUDY
OF THE SELF-SIMILARITY CONCEPT

Rein Tamsalu and Kai Myrberg

A ONE-DIMENSIONAL THERMODYNAMIC AIR-ICE-WATER MODEL:
TECHNICAL AND ALGORITHM DESCRIPTION REPORT

Bin Cheng and Jouko Launiainen

LITERATURE REVIEW ON MICROBIOLOGY OF AGGREGATES
ORIGINATING FROM PHYTOPLANKTON BLOOMS

Susanna Hietanen

MERI – Report Series of the Finnish Institute of Marine Research No. 37, 1998

Cover photo: Functioning test of a meteorological mast on the sea ice
in the Gulf of Bothnia during the Baltic Air-Sea-Ice Study (BASIS-98) (photo: P. Kosloff)

Publisher:
Finnish Institute of Marine Research
P.O. Box 33
FIN-00931 Helsinki, Finland
Tel: + 358 9 613941
Fax: + 358 9 61394 494
e-mail: surname@fimr.fi

Julkaisija:
Merentutkimuslaitos
PL 33
00931 Helsinki
Puh: 09-613941
Telekopio: 09-61394 494
e-mail: sukunimi@fimr.fi

Copies of this Report Series may be obtained from the library of the Finnish Institute of Marine Research.

Tämän raporttisarjan numeroita voi tilata Merentutkimuslaitoksen kirjastosta.

ISSN 1238-5328

Tummavuoren Kirjapaino Oy, Vantaa 1998

CONTENTS

A THEORETICAL AND EXPERIMENTAL STUDY OF THE SELF-SIMILARITY CONCEPT

Rein Tamsalu[1,2] and Kai Myrberg[2]

[1]Estonian Marine Institute, Paldiski Road 1, EE 00001 Tallinn, Estonia
[2]Finnish Institute of Marine Research, P.O. Box, 33, 00931, Helsinki, Finland

ABSTRACT

Both a theoretical and an experimental study of the self-similarity concept is carried out. Self-similarity means that a non-dimensional marine system variable (e.g. temperature) can be described as dependent on a non-dimensional vertical coordinate only. The theory is extended, and an expression is found for the non-dimensional vertical flux of temperature (flux self-similarity). An analysis of CTD soundings carried out at a station in the Baltic Sea supported the theory. It is clearly shown that the self-similar profiles are strongly dependent on the evolution of the mixed layer depth. Hence, different profiles are found in cases of detrainment and entrainment. In terms of the self-similarity concept, the coefficient for vertical turbulent diffusion can be found.

Keywords: non-dimensional, self-similarity concept, flux self-similarity, mixed layer evolution

INTRODUCTION

The self-similarity concept in the marine sciences was first introduced more than twenty years ago by Kitaigorodskii & Miropolski (1970). They found that a non-dimensional temperature is only dependent on a non-dimensional vertical coordinate. Since that work, many investigations have been devoted to studying the self-similarity concept. Miropolski & al. (1970) found average monthly dimensionless profiles for the two ocean stations Papa and Tango. Reshetova & Chalikov (1977) extended the self-similarity hypothesis for salinity. Linden (1975) carried out laboratory investigations using a rectangular tank with a two-layer vertical structure. A non-dimensional vertical structure for density was found. Mälkki & Tamsalu (1985), using the measured data of Nõmm (1988), found that the self-similarity profile strongly depends on the evolution of the mixed layer thickness. There are two different self-similarity structures: firstly, the case of entrainment when the homogeneous layer is deepening (storm in progress) and secondly, the case of detrainment when the mixed layer is decreasing (storm subsiding). In a real situation these two profiles are mixed, so the observations lie between these two curves.

Zilitinkevich & Mironov (1992) studied vertical fluxes through the thermocline. They developed a model of heat transfer in the thermocline from considerations of the turbulent energy budget and from expressions for effective heat conductivity, which is based on dimensional arguments using the buoyancy parameter, temperature gradient and turbulent length scale as governing parameters. This energy balance model is applicable to the deepening mixed layer as well as to its steady state and collapse.

The physical background of self-similarity has been investigated by several scientists. Barenblatt (1978) concluded that in the case of an increasing mixed layer, the thermocline is treated as a quasistationary thermal and diffusion wave. It is likely that the energy needed to erode the sharp gradient below the surface layer in the upper thermocline is supplied by the breaking of internal waves. Zilitinkevich & Rumjantsev (1990) have extended the theory by taking the effects of buoyancy into account.

In the present paper an experimental support for both the traditional self-similarity and the flux self-similarity concepts is shown using the CTD vertical profiles (about 80 in number), which were recorded at a station in the Baltic Sea during an expedition of R/V Aranda in July 1995.

In the next section, the experiment will be described, as well as the methods used for data analysis. The theoretical background for flux self-similarity is introduced, too. In the second section, the self-similar

profiles will be shown and the results of the analyses of experimental data will be compared with theory. In the last section, the main conclusions of the study will be given.

The reader interested in self-similarity in more detail is referred to the papers of Barenblatt (1996) and Tamsalu & al. (1997).

1. MATERIAL AND METHODS

1.1 Theoretical derivation of the flux self-similarity

The vertical structure of temperature in the seasonal thermocline will be written in the following form:

$$\frac{\partial T}{\partial t} = -\frac{\partial q}{\partial z} \tag{1}$$

where:

T(z,t) is the temperature, $q = \langle w' T' \rangle$ is the temperature flux, t is time, z is the vertical coordinate directed downwards. Substituting the non-dimensional coordinate:

$$\varsigma = \frac{z - h(t)}{H - h(t)} \tag{2}$$

equation (1) can be written as follows:

$$(H-h)\frac{\partial T}{\partial t} - (1-\varsigma)\frac{\partial h}{\partial t}\frac{\partial T}{\partial \varsigma} = -\frac{\partial q}{\partial \varsigma} \tag{3}$$

where:

h(t) is the thickness of the upper mixed layer and H is the bottom of the seasonal thermocline. The following expression for the non-dimensional temperature (θ) and for the non-dimensional temperature flux (Q) are proposed:

$$\theta = \frac{T_1(t) - T(t,z)}{T_1(t) - T_H} \tag{4}$$

$$Q = \frac{q_h(t) - q(t,z)}{q_h(t) - q_H} \tag{5}$$

where:

$T_1(t)$ is the temperature in the upper mixed layer, T_H is the temperature at the bottom of the seasonal thermocline (z=H), $q_h(t)$ is the temperature flux at the level z=h, q_H is the temperature flux at the level z=H. Here we suppose that $q_h(t) >> q_H$. Then (5) can be written as follows:

$$Q = \frac{q_h(t) - q(t,z)}{q_h(t)} \tag{5a}$$

Using (4) and (5a), equation (3) takes the form:

$$(1-\theta)a_1 - (1-\varsigma)\frac{\partial \theta}{\partial \varsigma}a_2 = \frac{\partial Q}{\partial \varsigma} \tag{6}$$

where:

$$a_1 = \frac{H-h}{q_h}\frac{\partial T_1}{\partial t} \;;\; a_2 = \frac{T_H - T_1}{q_h}\frac{\partial h}{\partial t}$$

If a_1 and a_2 are constants, then θ and Q are functions of ς only. We start to investigate this problem from equation (3). Vertically integrating (3) with respect to ς between the limits of 0 and 1, we get:

$$(H-h)\frac{\partial \overline{T}}{\partial t} - (\overline{T} - T_1)\frac{\partial h}{\partial t} = q_h \tag{7}$$

where:

$$\overline{T} = \int_0^1 T d\varsigma$$

The double integration, first between the limits of 0 and ς and then between the limits of 0 and 1 gives the following results:

$$(H-h)\frac{\partial \widetilde{T}}{\partial t} - (2\widetilde{T} - T_1)\frac{\partial h}{\partial t} = q_h - \overline{q} \tag{8}$$

where:

$$\widetilde{T} = \int_0^1 d\varsigma \int_0^{\varsigma} T d\varsigma \quad \text{and} \quad \overline{q} = \int_0^1 q d\varsigma$$

Using the relationship:

$$\frac{2\widetilde{T} - T_1}{\overline{T} - T_1} = \alpha_0 \tag{9}$$

we get from (7) and (8) the following equation:

$$a_1 - \frac{\alpha_0}{1-\alpha_0} a_2 = \frac{2-\alpha_0}{1-\alpha_0} - \frac{2}{1-\alpha_0}\beta_0 \tag{10}$$

where:

$$\kappa = \frac{\overline{T} - T_1}{T_H - T_1} \;;\; \beta_0 = \frac{\overline{q}}{q_h}$$

For the determination of q_h we use the well-known relationship for entrainment (Phillips 1977) in the form:

$$q_h = -c_0^{-1}(\overline{T} - T_1)\frac{\partial h}{\partial t} \tag{11}$$

where:

c_0 is a proportionality constant. Using (11) a_2 takes the form:

$$a_2 = -\frac{c_0}{\kappa} \tag{12}$$

Equation (10) then takes the form:

$$a_1 = (2 - \alpha_0(1 + c_0) - 2\beta_0)/(1 - \alpha_0) \tag{13}$$

We continue the study using analyses of experimental data together with the relationship for the vertical structure of the heat flux in the form:

$$q\frac{dT}{dz} = -\chi\left\langle\left(\frac{\partial T'}{\partial z}\right)^2\right\rangle \tag{14}$$

where:

χ is the molecular heat conductivity, T' is the fluctuation in temperature for each profile, $\langle\ \rangle$ is ensemble average.

Equation (14) was proposed by Osborn & Cox (1972).

1.2 The cruise

A cruise of R/V Aranda was carried out in July 1995 in order to collect the experimental data used in this study. The cruise took place in the Baltic Sea, in the western part of the Gulf of Finland at station JML (59°34'N, 23°37'E), where the sea depth is about 78 m. The measurements were started on July 24 at 13 GMT and ended on July 28 at 03 GMT (with a break between 08 GMT and 15 GMT on July 26). CTD measurements of temperature and conductivity, from which salinity and buoyancy were calculated, were carried out at 1-hour intervals using a SIS plus 500 CTD profiler (SIS=Sensoren-Instrumente-System). The measurements were collected at a depth interval of 0.1 metres.

The measurements at station JML showed that there was a clear well-mixed layer with a mean depth of about 11.5 m. Below that, a sharp thermocline existed. The largest vertical temperature changes took place in the layer between 15 and 25 m. Below 35 m the vertical temperature changes were negligible (Fig. 1).

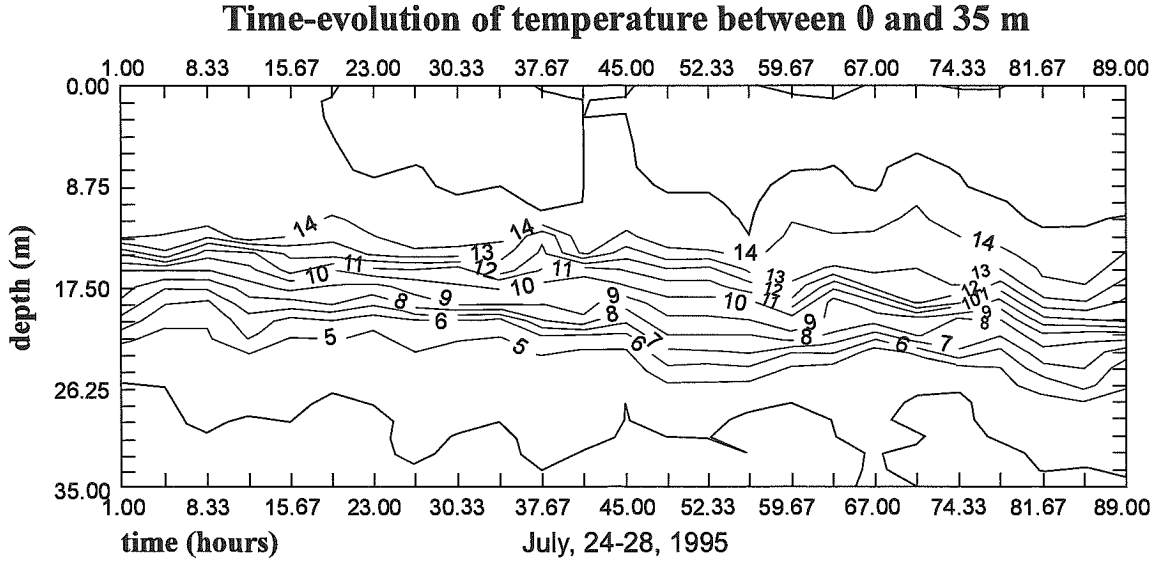

Fig. 1. The time evolution of temperature at depths between 0 and 35 m during the cruise. The x-axis is the time in hours from the beginning of the cruise. The y-axis is the depth; the isoline analysis has been carried out for temperature at an interval of 1°C.

1.3 Analysis of the measurements

In the analysis of all the 81 vertical profiles the following procedure was carried out separately for each profile. Firstly, attention was only directed at levels down to the lower limit of the thermocline (35 m), below which the temperature gradient was negligible. The depth of the mixed layer was calculated using

the criteria that the bottom of the upper mixed layer occurred where $\frac{\partial T}{\partial z} > 0.1^{\circ}\,C/m$. After that, the non-dimensional vertical coordinate ς was calculated for every depth (at intervals of 0.1 metres):

The non-dimensional vertical coordinate ς was taken at intervals of 0.01 ($0 \le \varsigma \le 1$) for all profiles by using (2) and the known parameters z, h(t) and H. The corresponding value of temperature with respect to ς was then chosen. The non-dimensional temperature θ can then be calculated using (4).

The next step was to calculate the vertical structure of the heat flux $q = \langle w' T \rangle$ from the CTD measurements using (14).

Two types of vertical structure of temperature fluctuations are found. In case A, the vertical temperature fluctuation gradient $\frac{dT'}{dz}$ has a maximum value at the interface between the mixed layer and the stratified layer. In case B, $\frac{dT'}{dz} = 0$ at the interface, and the maximum of the gradient occurs at a level approximately 1/4 of the total depth of the stratified layer. We have used these criteria to separate the profiles. In the first case (A), the mixed layer is increasing and in the second case (B) the mixed layer is decreasing. These two cases also become visible in the analysis of the measurements: we found 61 case-A profiles, and 20 case-B profiles. The bottom of the stratified layer was defined as being at the depth where the vertical temperature fluctuation gradient $\frac{dT'}{dz} = 0$. According to the measurements, this level was at a depth of 35 m. It becomes clear from Figure 1 that the depth of the mixed layer was increasing during the experiment.

2. RESULTS

In the following we will study the self-similar profiles separately for entrainment (case A) and for detrainment (case B). However, the main scientific interest here is focused on case A, both because of the small number of observations in case B and also because of the partly unknown physics behind detrainment.

The non-dimensional temperature θ calculated according to the measurements is shown plotted against the non-dimensional vertical co-ordinate ς (Fig. 2) separately for case A (Fig. 2a), in which the mixed layer depth is increasing and for case B (Fig. 2b), in which the mixed layer depth is decreasing. The continuous lines in Figures 2a and 2b represent the theoretical self-similar profiles calculated from (15) for case A and from (16) for case B (see below). The dotted lines represent the results of measurements. Equations (15) and (16) take the form (see Mälkki & Tamsalu 1985):

$$\theta(\varsigma) = 1 - (1-\varsigma)^3 \quad ;\ \text{case A} \tag{15}$$

$$\theta(\varsigma) = 1 - 4(1-\varsigma)^3 + 3(1-\varsigma)^4 \quad ;\ \text{case B} \tag{16}$$

It is clear that the profiles for cases A and B differ from each other, not surprisingly, because different physical mechanisms lie behind them. In case A ($\frac{\partial h}{\partial t} > 0$) the experimental data seem to fit quite well with the theory; the conclusion appears to be that there is a self-similar structure for temperature. On the other hand, in case B (20 observations, $\frac{\partial h}{\partial t} \le 0$), due to the quite small number of observations, the single experimental curves (dotted lines) have quite a large scatter. Another possible reason for the scatter is that there is a continuous change in the evolution of the mixed layer, i.e. a change from a type-B profile to a type-A profile and vice versa. Some profiles do actually represent a transition between types A and B. Most of the time, type-A profiles dominated and only 25 percent of the profiles were of type B. Most

probably, some of these were not "pure" type-B profiles, which is shown by the large scatter of the latter curves. The 61 type-A curves (Fig. 2a) show a better fit with the theoretical curve and less scatter compared to case B. This is clear, because the number of profiles is large and most of the time the mixed layer evolution was of type-A.

The above analysis of the results shows that the self-similar profile (type A or B) of temperature is not so clearly visible instantaneously. Mälkki & Tamsalu (1985) pointed out that κ only reaches a constant value if an integration over the inertial period (about 14 hours) is carried out.

The vertical flux of temperature $\langle w'T' \rangle$ has been calculated according to (14). The fluxes are presented separately for cases A and B as a function of ς. The most striking feature is that the shapes of the flux profiles differ clearly from each other. In case A the flux has its maximum value near $\varsigma = 0$ and decreases towards $\varsigma = 1$ (Fig. 3a), while in case B (Fig. 3b), the maximum flux is reached between $\varsigma = 0.2 - 0.3$, decreasing again towards $\varsigma = 1$.

After deriving the vertical flux of temperature $\langle w'T' \rangle$, a vertical integration of the experimentally-derived profiles is carried out. We investigate here only case A.

The calculated values of α_0 lie between 0.69-0.82, and we take α_0=0.75. The calculated β_0 was 0.61, and we take β_0=0.6. The calculated values of κ lie between 0.72-0.77, and we take κ=0.75. This can also be found by integrating (4) using (15):

$$\int_0^1 \theta d\varsigma = \frac{T_1(t) - \overline{T}(t)}{T_1(t) - T_H} = \kappa \tag{17}$$

Integrating (6) with respect to ς, we get:

$$\left(\varsigma - \int_0^{\varsigma} \theta d\varsigma\right) a_1 - ((1-\varsigma)\theta + \int_0^{\varsigma} \theta d\varsigma) a_2 = Q \tag{18}$$

Integrating (6) between the limits of 0 and 1, we get:

$$(1-\kappa)a_1 - \kappa a_2 = 1 \tag{19}$$

Substituting the values of α_0, β_0 and κ into (12) and (13) we find, using (19), that c_0=3.8,

$$a_1 = -11.2 \text{ and } a_2 = -5.07 \tag{20}$$

Substituting (15) and (20) into (18) we get the following expression for the temperature flux Q:

$$Q = 1 - (1-\varsigma)^4 \tag{21}$$

The temperature flux can be written in the traditional way as follows:

$$q = -\nu \frac{\partial T}{\partial z} \tag{22}$$

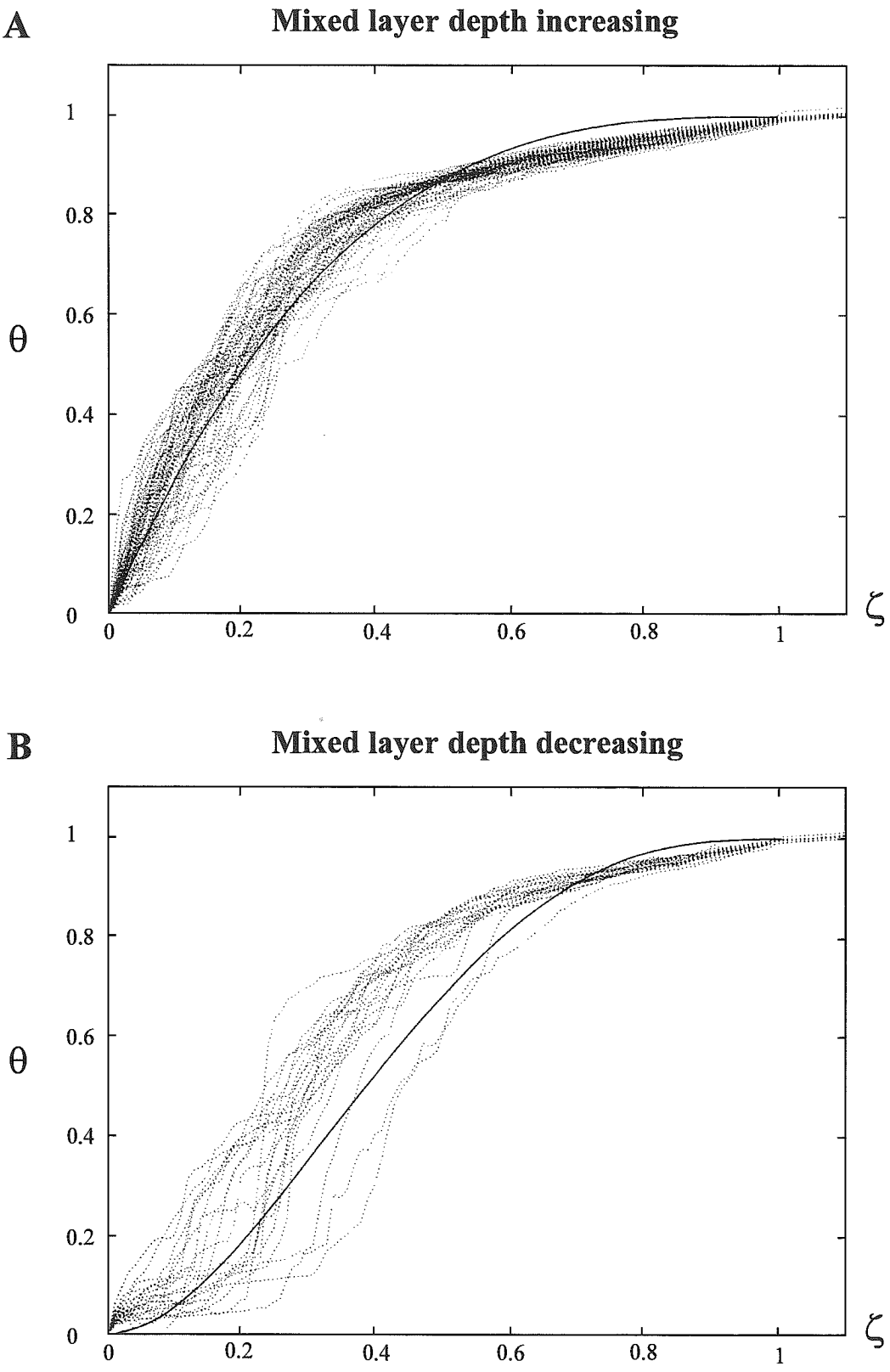

Fig. 2. The non-dimensional temperature θ plotted against the non-dimensional vertical coordinate ς. The curves based on observations are marked with dotted lines. The theoretical curves are marked with continuous lines: A -the mixed layer depth is increasing, B -the mixed layer depth is decreasing.

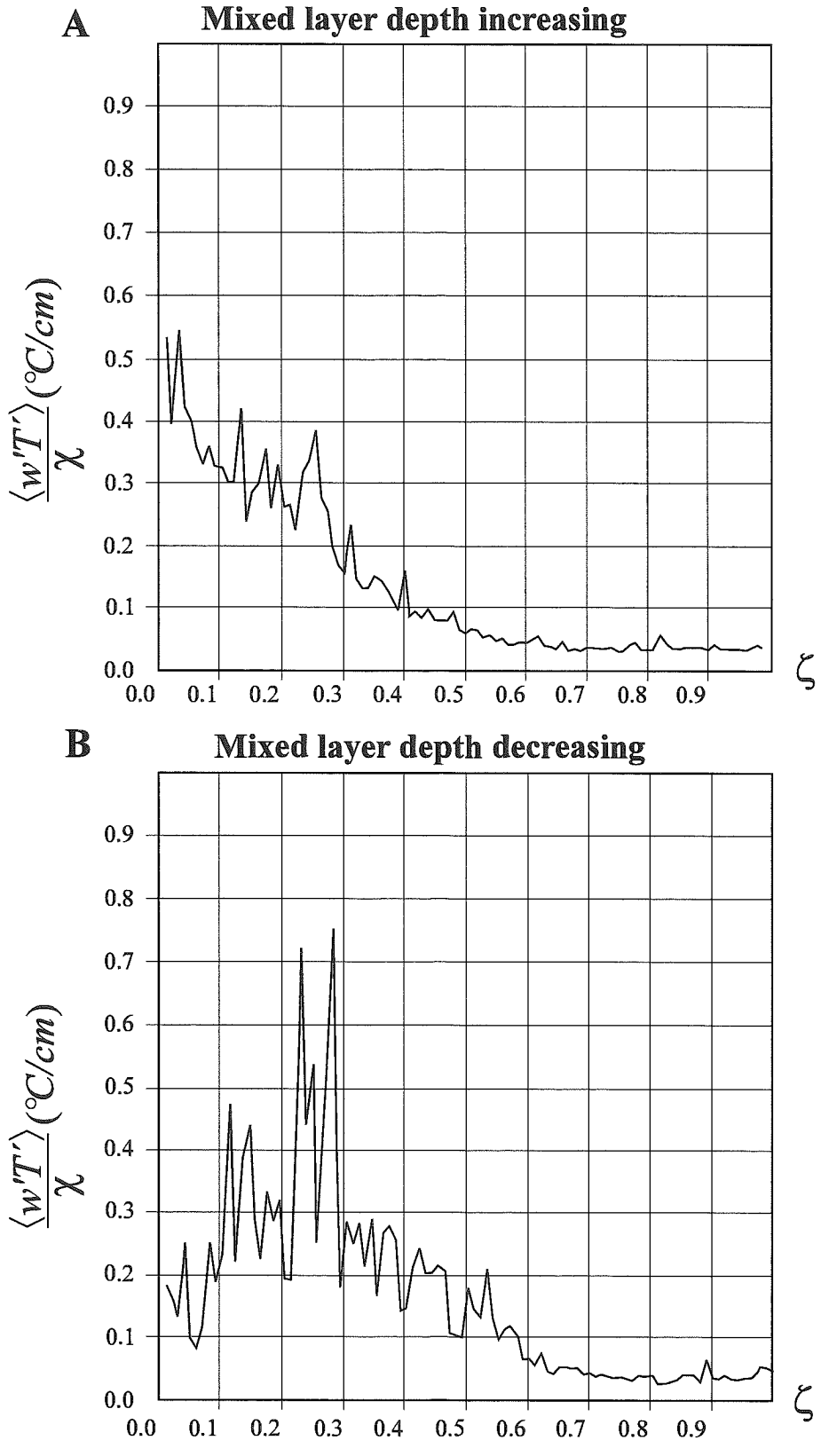

Fig. 3. The vertical flux of temperature $\frac{\langle w' T' \rangle}{\chi}$ plotted against the non-dimensional vertical coordinate ς. The flux is calculated according to (3): A -the mixed layer depth is increasing, B -the mixed layer depth is decreasing.

Using (15), (21) and (22) we get the following equation for the coefficient of vertical turbulent diffusion ν:

$$\upsilon = -\frac{1}{2}(1-\varsigma)^2 \frac{H-h}{a_2}\frac{\partial h}{\partial t} = 0.1*(H-h)\frac{\partial h}{\partial t}(1-\varsigma)^2 \qquad (23)$$

If the diurnal change in the upper mixed layer thickness is 1 m, and the thermocline thickness is 30 m, then:

ν=0.3 cm^2/s

at the top of the thermocline.

For practical use, equations (23) and (9) are the most important ones.

The non-dimensional vertical fluxes of temperature as a function of the non-dimensional vertical co-ordinate ς are presented in Figure 4. The theoretical curve corresponding to (21) is marked Q_2 in case A (Fig. 4a). The experimental non-dimensional vertical flux is marked as Q_1. The corresponding approximate curves for detrainment (case B) are shown in Figure 4b. A comparison of the experimental results with theory has the same main features as in the case of the traditional self-similarity concept. In case A, the observations fit well with theory.

3. DISCUSSION AND CONCLUSIONS

The traditional self-similarity concept as well as the extended theory of self-similarity of vertical fluxes were compared with calculations based on an analysis of observations. In general, the observations supported the theory. However, the four-day expedition was far too short to gather an adequate data set of CTD profiles in different stability conditions of the air-sea interface with respect to the evolution of the mixed layer thickness.

The self-similar profiles for temperature based on the observations showed that different kinds of profiles exist depending on the evolution of the mixed layer, with different profiles being found for cases of entrainment (case A) and detrainment (case B). The observational proof for the self-similar structure of temperature was better in case A, while the profiles representing case B gave less satisfactory evidence. This is partly because of the small number of case-B profiles measured. On the other hand, most of the time case A conditions dominated, and profiles representing case B were not always pure; i.e. some profiles represented the transition between detrainment and entrainment. However, self-similarity of temperature becomes visible if a time-integration over an inertial period (about 14 h) is carried out (see Mälkki & Tamsalu 1985).

The profiles of the vertical temperature fluxes showed a clear difference between cases A and B. The non-dimensional fluxes of temperature also showed differences in the profiles based on the evolution of the mixed layer depth. In case A, the fit of theory with observations was better than in case B, the reasoning for this being the same as in the case of the self-similarity profile for temperature.

In the case of an entrainment type of profile, the coefficient of vertical turbulent diffusion can be solved in the stratified layer using the flux-self-similarity concept. Thus, the self-similarity concept can be used as a tool to parameterize the vertical turbulence in numerical modelling.

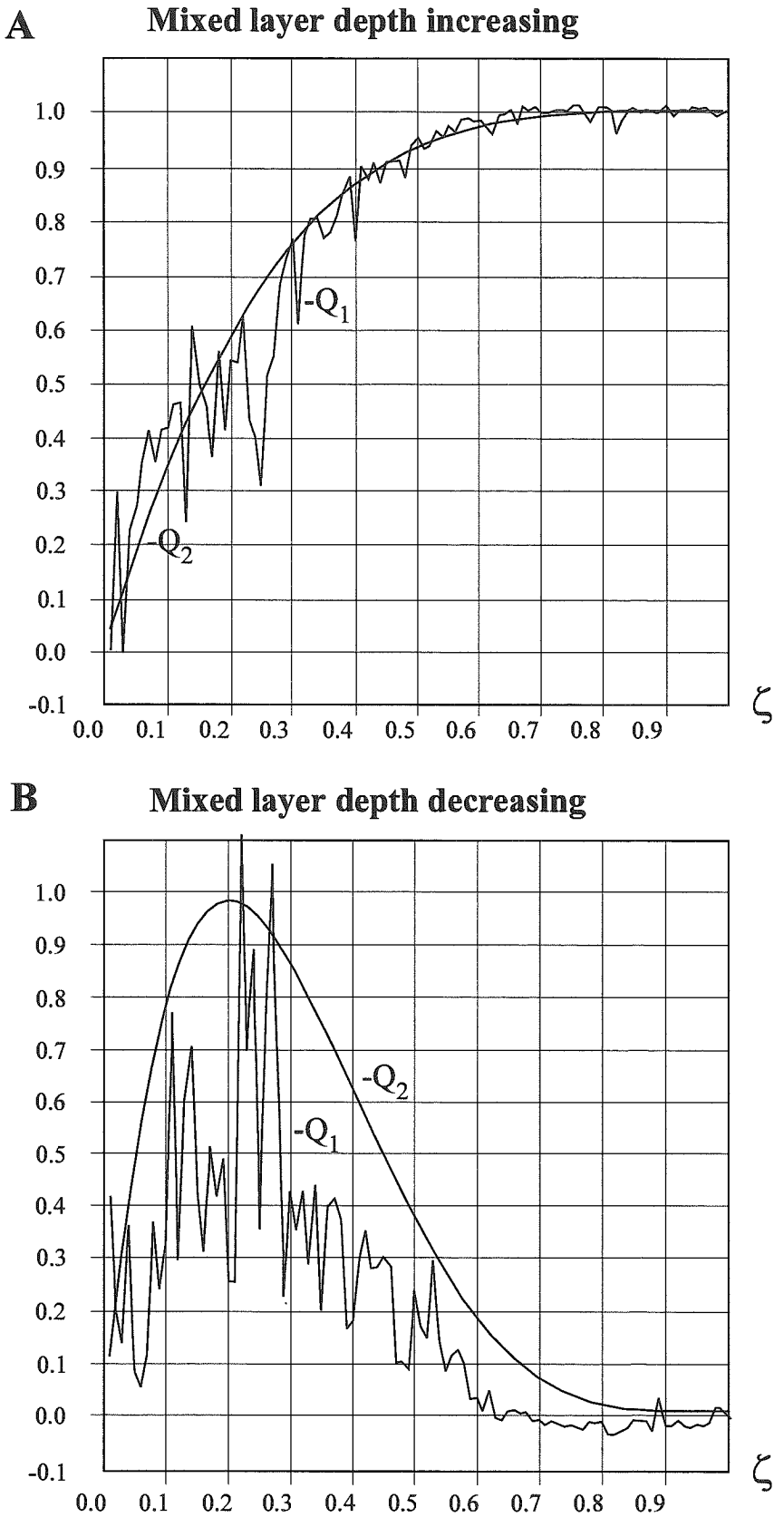

Fig. 4. The non-dimensional vertical flux of temperature Q plotted against the non-dimensional vertical coordinate ς. Curve Q_1 is based on experimental results, while curve Q_2 is based on theoretical calculations: A -the mixed layer depth is increasing, B -the mixed layer depth is decreasing.

REFERENCES

Barenblatt, G. 1978: Self-similarity of temperature and salinity distributions in the upper thermocline. - Izv., Atmospheric and Oceanic Physics, No. 11, 820-823 (English edition).

Barenblatt, G. 1996: Scaling, self-similarity, and intermediate asymptotics. - Cambridge texts in applied mathematics, Cambridge University Press, U.K., 386 pp.

Kitaigorodskii, S. & Miropolski, Y. 1970: On the theory of the open-ocean active layer. - Izv., Atmospheric and Oceanic Physics, 6, No. 2, 178-188 (English edition).

Linden, P. 1975: The deepening of a mixed layer in a stratified fluid. - J. Fluid. Mech., 71, part 2, 385-405.

Miropolski, Y., Filyushkin, B. & Chernyskov, P. 1970: On the parametric description of temperature profiles in the active ocean layer. - Oceanology, 10, No. 6, 892-897 (English edition).

Mälkki, P. & Tamsalu, R. 1985: Physical features of the Baltic Sea. - Finnish Mar. Res. No. 252, 110 pp., Helsinki.

Nõmm, A. 1988: The investigation and simulation of the thermohaline structure in the open part of the Gulf of Finland. - PhD-thesis, Leningrad Hydrometeorological Institute, 242 pp. (in Russian).

Osborn, T. & Cox, C. 1972: Oceanic fine structure. - Geophys. Fluid Dyn., 3, No. 5, 265-354.

Phillips, O. 1977: Entrainment. - In: modelling and prediction of the upper layers of the Ocean (Kraus, E.B.) Pergamon Press, Oxford, pp. 92-101.

Reshetova, O. & Chalikov, D. 1977: Universal structure of the active layer in the ocean. - Oceanology, 17, No. 5, 509-511 (English edition).

Tamsalu, R., Mälkki, P. & Myrberg, K. 1997: Self-similarity concept in marine system modelling. - Geophysica, 33(2): 51-68.

Zilitinkevich, S.S. & Rumjantsev, V. 1990: A parameterized model of the seasonal temperature changes in lakes. - Environmental Software, Vol. 5, No. 1, 12-25.

Zilitinkevich, S.S. & Mironov, D. 1992: Theoretical model of the thermocline in a freshwater basin. - J. Phys. Oceanogr., Vol. 22, No. 9, 988-994.

A ONE-DIMENSIONAL THERMODYNAMIC AIR-ICE-WATER MODEL: TECHNICAL AND ALGORITHM DESCRIPTION REPORT

Bin Cheng and Jouko Launiainen

Finnish Institute of Marine Research, P.O. Box 33, 00931, Helsinki, Finland

ABSTRACT

The technical description of a one-dimensional thermodynamic air-ice-sea model (Launiainen & Cheng, 1998) is given. Parameterizations, solution method, algorithm and program flow are reported. The model produces the ice thickness variation as well as the in-ice temperature profiles, air-ice surface fluxes and the atmospheric near-surface profiles of wind, temperature and moisture.

Keywords: air-ice coupling, air-ice-water fluxes, ice thermodynamics, numerical methods

INTRODUCTION

This report gives the technical description of a one-dimensional air-ice-water mass and energy balance model. The model includes the calculation of the air-ice interface temperature and surface fluxes, as well as the heat conduction in the snow and ice, and the heat flux and ice thickness variations at the ice-water boundary. In addition, the model yields the time development of the in-ice temperature profile and the atmospheric near-surface profiles of wind, temperature and moisture. Via the latter parameters, the model can be dynamically coupled with atmospheric boundary layer (ABL) models, for example.

The model is based on the heat conduction equation in the snow and ice, in which the diffusive and convective components of the heat and mass fluxes are approximated with a conservative difference numerical scheme derived using the integral interpolation method. The scheme can be adjusted upon request from explicit to implicit by a single parameter. In our model the implicit form is used, i.e. no restrictions upon the ratio of the space and time steps are necessary and the scheme remains absolutely stable. In practice, the model contains an adaptive time step varying from 10^{-1} hour upwards. Short time steps (0.1 h) are associated primarily with process studies and with studies of air-ice interaction, while longer time steps (e.g. 6h) are associated with climatological studies. The overall structure of the model is flexible, permitting an arbitrary number of nodal subdivisions and layers. Usually, the column of snow + ice is divided into 10 to 30 layers, even more if desired. The upper boundary condition is defined by the surface heat balance, and the lower boundary remains at the freezing point.

The governing equations at the air-ice interface are subject to meteorologically controlled boundary conditions. The surface fluxes are computed from user-given (files) observations of wind speed, air temperature, relative humidity and snowfall and, if available, of measured values of solar radiation. At the ice-water interface the flux from the water is given or estimated by a bulk formula. Various physical coefficients and parameterizations such as albedo, heat conductivity and ice and snow density, can be modified by user-defined parameters in files and by algorithm alterations. The model can be applied to calculation of thermodynamic ice growth, to air-ice and ice-ocean model coupling and to the combination of thermodynamic and dynamic ice models.

The physical details of the model are discussed in Launiainen & Cheng (1998). In the present report, the physical parameterizations and coefficients are listed, and the model solution method, algorithm and program flow descriptions are given.

BASIC EQUATIONS OF THE MODEL

The surface heat balance, the heat conduction through snow and ice, and the heat flow through the ice-water interphase are the processes which are involved in the model. Additionally, the atmospheric surface layer is dynamically coupled with the model via the flux-profile relationships of the turbulent fluxes of momentum, heat and moisture. The heat fluxes for an ice layer are shown in Fig. 1.

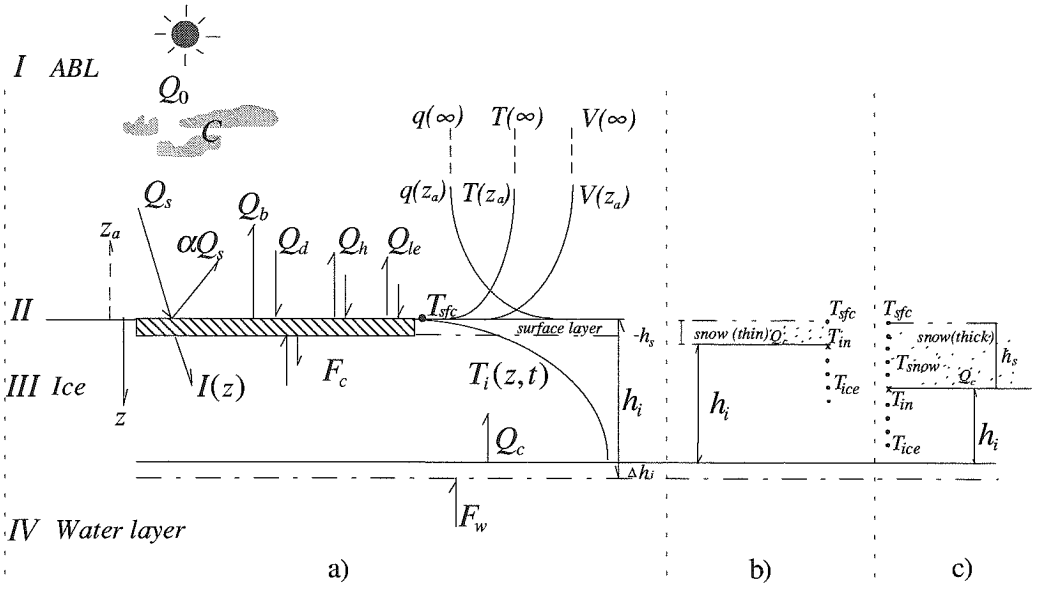

Fig. 1. a) Heat fluxes and notations (see list of symbols) for an ice layer. The schematic profiles in the atmospheric boundary layer (ABL) represent wind $V(z)$, temperature $T(z)$ and moisture $q(z)$. b) and c) give the definition in cases of thin and thick snow, respectively.

The basic model equations with respect to the various phases are summarized as follows:

I) In the ABL:

The profile gradients and profiles of wind speed, temperature and moisture are defined by the equations given by the Monin-Obukhov similarity theory, i.e. in terms of the universal profile gradients of

$$\frac{\partial V}{\partial z}\frac{k_0 z_a}{u_*} = \Phi_M(z_a/L); \quad \overset{integration}{\Rightarrow} \quad V(z_a);$$

$$\frac{\partial T}{\partial z}\frac{z_a}{\theta_*} = \Phi_H(z_a/L); \quad \overset{integration}{\Rightarrow} \quad T(z_a);$$

$$\frac{\partial q}{\partial z}\frac{z_a}{q_*} = \Phi_E(z_a/L); \quad \overset{integration}{\Rightarrow} \quad q(z_a);$$

In the above, the scaling parameters are defined as

$$u_* = \left(\frac{\tau}{\rho_a}\right)^{\frac{1}{2}}; \qquad \theta_* = \frac{Q_h}{\rho_a \cdot c_p \cdot k_0 \cdot u_*}; \qquad q_* = \frac{Q_{le}}{\rho_a \cdot k_0 \cdot u_*}$$

Physically, the variable z_a/L is dependent on u_*, θ_* and q_* (i.e. on the fluxes of momentum τ, sensible heat Q_h and latent heat Q_{le}) and the solution is iterative. In practice, the iteration is avoided by

using a relationship between z_a/L and a directly-calculable parameter the bulk-Richardson number, R_z, as $z_a/L = f(R_z)$ (Launiainen, 1995).

II) At the surface:

incoming short-wave radiation $Q_s = Q_s(\varphi, e, t, C)$

penetrating short-wave radiation $I(z,t) = (1-\alpha_{i,s}) \cdot Q_s(t) \cdot e^{-\kappa_{i,s} \cdot z}$

atmospheric long-wave radiation $Q_d = Q_d(T_a, e)$

surface-emitted long-wave radiation $Q_b = Q_b(T_{sfc})$

sensible heat flux $Q_h = -\rho_a \cdot c_p \cdot C_H \cdot (T_{sfc} - T_z) \cdot V_z$

latent heat flux $Q_{le} = -\rho_a \cdot R_l \cdot C_E \cdot (q_s - q_z) \cdot V_z$

bulk coeff. for heat $C_H = C_{Hz}(z_a, z_0, z_T, \Phi_M(z_a/L), \Phi_H(z_a/L))$

bulk coeff. for water vapour $C_E = C_{Ez}(z_a, z_0, z_q, \Phi_M(z_a/L), \Phi_E(z_a/L))$

cond. heat flux at air-ice interface $F_c = -\left(-k_{i,s} \dfrac{\partial T_{i,s}}{\partial z}\right)_{sfc}$

surface heat balance:

$$(1-\alpha)(1-e^{-\kappa_{i,s}\Delta h_{i,s}})Q_s + Q_d - Q_b(T_{sfc})_s + Q_h(T_{sfc}) + Q_{le}(T_{sfc}) + F_c(T_{sfc}) + F_m(T_f) = 0$$

surface heat balance given in terms of surface temperature dependent and non-dependent terms:

$$F(T_{sfc}) = \sum F_Q + \sum F_Q(T_{sfc}) = 0$$

heat used for melting in cases of $T_{sfc} \geq T_f$:

$$-\rho_{i,s} L_{if,sf}\, dh_{i,s}/dt = F_m(T_f)$$

III) In snow and ice:

conservation of heat in ice and snow $(\rho c)_{i,s} \dfrac{\partial T_{i,s}(z,t)}{\partial t} = -\dfrac{\partial}{\partial z}\left(-k_{i,s} \dfrac{\partial T_{i,s}(z,t)}{\partial z} + q(z,t)\right)$

surface temperature condition $T_{i,s}(0,t) = T_{sfc}(t)$

temperature at ice-water boundary $T_i(h_i, t) = T_b$

initial temperature profile $T_{i,s}(z,0) = T_{iso}(z)$

heat conduction in ice and snow $Q_c = -k_{i,s} \dfrac{\partial T_{i,s}}{\partial z}$

heat conduction at the snow-ice interface $k_s \dfrac{\partial T_s}{\partial z} = k_i \dfrac{\partial T_i}{\partial z}$

thickness of ice or snow $h_{i,s} = Q\left(F_m(T_f), Q_c(T_{i,s}), F_w(T_w, T_b)\right)$

IV) At the ice bottom, i.e. at the ice-water interface:

condition for freezing or melting $$-\rho_i \cdot L_{if} \cdot dh_i/dt = \left((-k_i\,\partial T_i/\partial z)_{bot} + F_w\right)$$

heat flux from water $$F_w = \rho_w c_w C_{HW}(T_w - T_f)W$$

STRUCTURE OF THE MODEL

(1) Vertical structure of the model

Generally, the overall structure of the model is flexible, permitting an arbitrary number of nodal sub-divisions, phases and layers. In our studies, two phases, i.e. snow and ice, are considered initially. The combined snow and ice column is normally divided into 10 to 30 layers, e.g. 10 layers of snow and 20 layers of ice, depending on the situation of these two phases.

The snow accumulation process is included in the model. If the snow cover is thin, it can be regarded as a single layer without an inner node (i.e. having a linear temp. profile), but the subdivision in the snow exists when the snow layer is thicker than 0.01m. For larger snow thickness, a linear temperature profile in the snow is assumed for the first few steps of the calculation. The vertical partition structure in the snow and ice layers is given in Fig. 2. The model is initialized with a (non-zero) thickness of ice and a profile of temperature in the snow and ice.

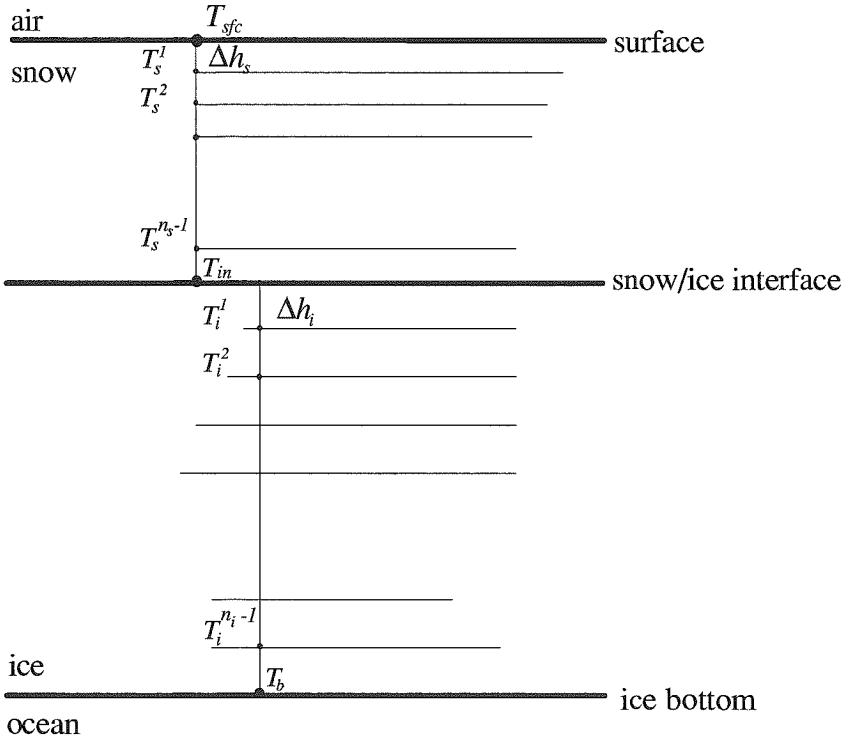

Fig. 2. The vertical structure of snow-ice system where n_s, n_i, are the total number of subdivision of snow and ice, respectively.

(2) The overall structure

The physical structure of the model is given in Fig. 3. The model is forced by the atmospheric input and by the heat flux from the water below, given the initial status of the snow and ice. The model is composed of several physical processes which are fully coupled with each other.

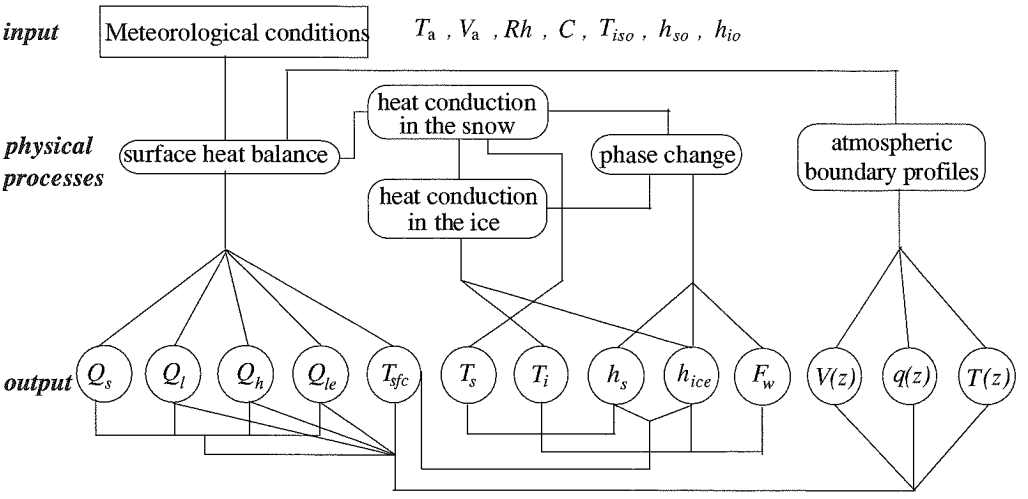

Fig. 3. Schematic overall structure between physical processes and the model output.

CALCULATION PROCEDURE, GRID AND FLOW DIAGRAM

(1) Solution of the matrix system

The basic equation of the conservation of heat in the ice and snow with the initial and boundary conditions can be written in the form

$$\rho c(z,t)\frac{\partial T(z,t)}{\partial t} - \frac{\partial}{\partial z}\left(k(z,t)\frac{\partial T(z,t)}{\partial z}\right) = Q(z,t) \qquad \text{(eq. c-1)}$$

$$T_{sfc}^{k} = T_{sfc}(t) \qquad \text{(eq. c-2)}$$

$$T_{n_i}^{k} = T_b \text{, and } T_{n_s}^{k} = T_{in} \qquad \text{(eq. c-3)}$$

$$T_j^0 = T_{iso}(z_j) \qquad \text{(eq. c-4)}$$

where $\rho c(z,t) = (\rho c)_{i,s}$, $k(z,t) = k_{i,s}$ and $\kappa_{i,s}\cdot(1-\alpha_{i,s})\cdot Q_s(t)\cdot e^{-\kappa_{i,s}z} = Q(z,t)$. Defining $z_j = j\cdot\Delta h_{i,s}$ and $j = 1,2,\cdots N-1$ and, $t_k = k\cdot\Delta t$ and $k = 1,2,3,\cdots$, where z and t denote the vertical space increase (positive downward below the surface) and time, respectively. $\Delta h_{i,s}$ and Δt are the space and time step, respectively. $N = n_{i,s}$ the total subdivision of snow or ice (cf. Fig. 2).

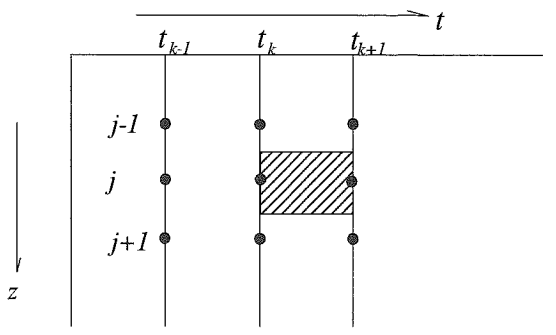

Fig. 4. Integration area (shaded) of the equation of conservation of heat given schematically in z and t coordination.

Based on the integral interpolation method (Cheng, 1996; Launiainen & Cheng, 1998) the equation above can finally be discretized to a system of difference equations. The integration area is given schematically in Fig. 4. This leads (cf. eq (B10) in Launiainen & Cheng, 1998) to the system:

$$-\frac{\Delta t\cdot\theta}{\Delta h}A_j^{k+1}T_{j-1}^{k+1}+\left[\frac{\Delta h}{2}\left(\rho c_j^{k+1}+\rho c_j^{k}\right)+\frac{\Delta t\cdot\theta}{\Delta h}\left(A_j^{k+1}+A_{j+1}^{k+1}\right)\right]T_j^{k+1}-\frac{\Delta t\cdot\theta}{\Delta h}A_{j+1}^{k+1}T_{j+1}^{k+1}=$$

$$-\frac{\Delta t\cdot(1-\theta)}{\Delta h}A_j^{k}T_{j-1}^{k}+\left[\frac{\Delta h}{2}\left(\rho c_j^{k+1}+\rho c_j^{k}\right)-\frac{\Delta t\cdot(1-\theta)}{\Delta h}\left(A_j^{k}+A_{j+1}^{k}\right)\right]T_j^{k}-\frac{\Delta t\cdot(1-\theta)}{\Delta h}A_{j+1}^{k}T_{j+1}^{k}$$

$$+Q_j^{k+1/2}\cdot\Delta t\cdot\Delta h$$

$$j=1,2,\cdots n_{i,s}-1,\ 0\le\theta\le 1.$$

where the A_j^k is approximate to $A_j^k\approx\frac{1}{2}\left(k_{i,s}(z_{j-1},t_k)+k_{i,s}(z_j,t_k)\right)$, $\rho c_j^k=\rho c_{i,s}(z_j,t_k)$ and

$$Q_j^{k+1/2}=\kappa\cdot(1-\alpha)\cdot Q_s(t_{k+1/2})\cdot e^{-\kappa\cdot z_j}.$$

Writing the group of equations in matrix form, we have

$$\overline{A}\,\overline{T}^{k+1}=\overline{B}\,\overline{T}^{k}+\overline{Q} \qquad \text{(eq. s-1)}$$

where

$$\overline{A}=$$

$$\begin{pmatrix}
\frac{1}{2}\left(\rho c_1^{k+1}+\rho c_1^{k}\right)+\frac{\Delta t\cdot\theta}{\Delta h^2}\left(A_1+A_2\right)^{k+1} & -\frac{\Delta t\cdot\theta}{\Delta h^2}A_2^{k+1} & 0 & 0\\
-\frac{\Delta t\cdot\theta}{\Delta h^2}A_2^{k+1} & \ddots & \ddots & 0\\
0 & \ddots & \ddots & -\frac{\Delta t\cdot\theta}{\Delta h^2}A_{N-1}^{k+1}\\
0 & 0 & -\frac{\Delta t\cdot\theta}{\Delta h^2}A_{N1}^{k+1} & \frac{1}{2}\left(\rho c_{N-1}^{k+1}+\rho c_{N-1}^{k}\right)+\frac{\Delta t\cdot\theta}{\Delta h^2}\left(A_{N-1}+A_N\right)^{k+1}
\end{pmatrix}_{(N-1)\times(N-1)}$$

$$\overline{B}=$$

$$\begin{pmatrix}
\frac{1}{2}\left(\rho c_1^{k+1}+\rho c_1^{k}\right)-\frac{\Delta t\cdot(1-\theta)}{\Delta h^2}\left(A_1+A_2\right)^{k} & \frac{\Delta t\cdot(1-\theta)}{\Delta h^2}A_2^{k} & 0 & 0\\
\frac{\Delta t\cdot(1-\theta)}{\Delta h^2}A_2^{k+1} & \ddots & \ddots & 0\\
0 & \ddots & \ddots & \frac{\Delta t\cdot(1-\theta)}{\Delta h^2}A_{N-1}^{k}\\
0 & 0 & \frac{\Delta t\cdot(1-\theta)}{\Delta h^2}A_{N-1}^{k} & \frac{1}{2}\left(\rho c_{N-1}^{k+1}+\rho c_{N-1}^{k}\right)-\frac{\Delta t\cdot(1-\theta)}{\Delta h^2}\left(A_{N-1}+A_N\right)^{k}
\end{pmatrix}_{(N-1)\times(N-1)}$$

$$\overline{Q}=\begin{pmatrix}
-\frac{\Delta t\cdot\theta}{\Delta h^2}A_1^{k+1}T_{sfc}^{k+1}+\frac{\Delta t\cdot(1-\theta)}{\Delta h^2}A_1^{k}T_{sfc}^{k}+\Delta t\cdot Q_1^{k+1/2}\\
\Delta t\cdot Q_2^{k+1/2}\\
\cdots\\
-\frac{\Delta t\cdot\theta}{\Delta h^2}A_N^{k+1}T_b^{k+1}+\frac{\Delta t\cdot(1-\theta)}{\Delta h^2}A_n^{k}T_b^{k}+\Delta t\cdot Q_{N-1}^{k+1/2}
\end{pmatrix}_{(N-1)\times 1}$$

and $\overline{T}^{k+1} = \begin{pmatrix} T_1^{k+1} \\ T_2^{k+1} \\ .. \\ .. \\ T_{N-1}^{k+1} \end{pmatrix}_{(N-1)\times 1}$, $\overline{T}^{k} = \begin{pmatrix} T_1^{k} \\ T_2^{k} \\ .. \\ .. \\ T_{N-1}^{k} \end{pmatrix}_{(N-1)\times 1}$

The elements of matrices $\overline{A}$, $\overline{B}$ and $\overline{Q}$ must be known before we use a speeded-up method to calculate $\overline{T}^{k+1}$ by the matrix equation. Actually, an iterative procedure is used, since A_j^k and ρc_j^k are functions of T_j^k.

$$\overline{A}(\overline{T}^k)\overline{T}^* = \overline{B}(\overline{T}^k)\overline{T}^k + \overline{Q} \qquad \text{(eq. it-1)}$$

$$\overline{A}(\overline{T}^*)\overline{T}^{*1} = \overline{B}(\overline{T}^*)\overline{T}^k + \overline{Q} \qquad \text{(eq. it-2)}$$

The basic process reads:

i) Calculate system matrices $\overline{A}$ and $\overline{B}$ with the current step value of $\overline{T}^k$ and current forcing data.

ii) Calculate $\overline{T}^*$ instead of $\overline{T}^{k+1}$ by the scheme (eq. it-1).

iii) Calculate system matrices $\overline{A}$ and $\overline{B}$ with $\overline{T}^*$.

iv) Calculate $\overline{T}^{*1}$ by the scheme (eq. it-2).

v) Repeat the step iii) and iv) until T^{*k} and $T^{*(k-1)}$ are close enough, i.e. $T^{*k} \approx T^{*(k-1)}$.

vi) Set the value of the next step, i.e. $\overline{T}^{k+1} = T^{*k}$ and repeat the procedure from i) with the next step's forcing data.

(2) Grid system

We have a grid system in our model in which the total number of inner nodes does not change (Lagrangian grid). Accordingly, the thicknesses of the snow and ice layers do not remain constant, and the grid coordinates vary with time. Fig. 5 shows an example of an ice layer with accretion and ablation from the bottom. The coordinate system moves with the surface which may itself change in the vertical, as well. The black dots are the grid points defined by the current time step while the horizontal line segments give the grid points as first defined, estimated by the previous time step.

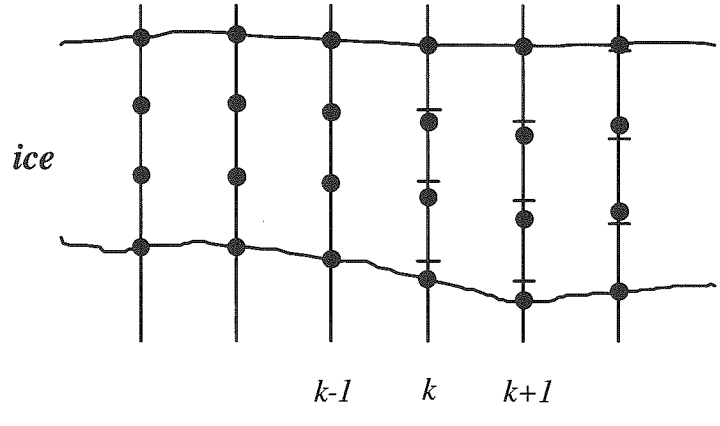

Fig. 5. Grid system of an ice layer with the moving boundary (with respect of time and thickness). The black dots are the grid points defined by the current step while the short segment give the grid points as defined by the previous step.

Because of the moving boundaries, a procedure similar to the initialization of the temperature profile is adopted to treat the inner moving node system :

i) temperature at each node of the previous step $k-1$ is known.

ii) calculate the total thickness variation at step $k-1$ and calculate each node position at step k.

iii) calculate the temperature (initial value) at each node at step k by a piecewise interpolation using the values given by the previous step $k-1$ (segment at step k)

iv) calculate the temperature (second value) at each node at step k by the forcing data.

v) repeat iv) until the temperature at each node for the step k remains stable. The temperature at each node for the current step k is then known.

(3) Flow diagram

The computer program is based on the flow diagram below (Fig. 6). The do loops k in the flow indicate the time development, and m is the iterative procedure for surface temperature. In practice, less than 5 steps are needed for the T_{sfc} calculation.

SUBROUTINES AND THE FORMULAE

The formulae used are summarized below. For further physical explanation and discussion, see Launiainen & Cheng (1998).

Water vapour pressure in the air (subroutine: wvap.f ; emb.f)

$\varepsilon = \exp((-6763.6/T) - 4.9283 \cdot \ln T + 54.23)$ $T > 273.15$ *Iribarne & Godson (1973)*

$\varepsilon = \exp((-6141/T) + 24.3)$ $T < 273.15$

if T_{dew} *is known*

$e = \varepsilon(T_{dew})$

if T_{wet}, T_{dry} *are known*

$e = \varepsilon(T_{wet}) - 0.666(T_{dry} - T_{wet})$ $T > 273.15$

$e = \varepsilon(T_{wet}) - 0.57(T_{dry} - T_{wet})$ $T < 273.15$

if Rh, T_a *are known*

$e = \varepsilon(T_a) \cdot Rh$

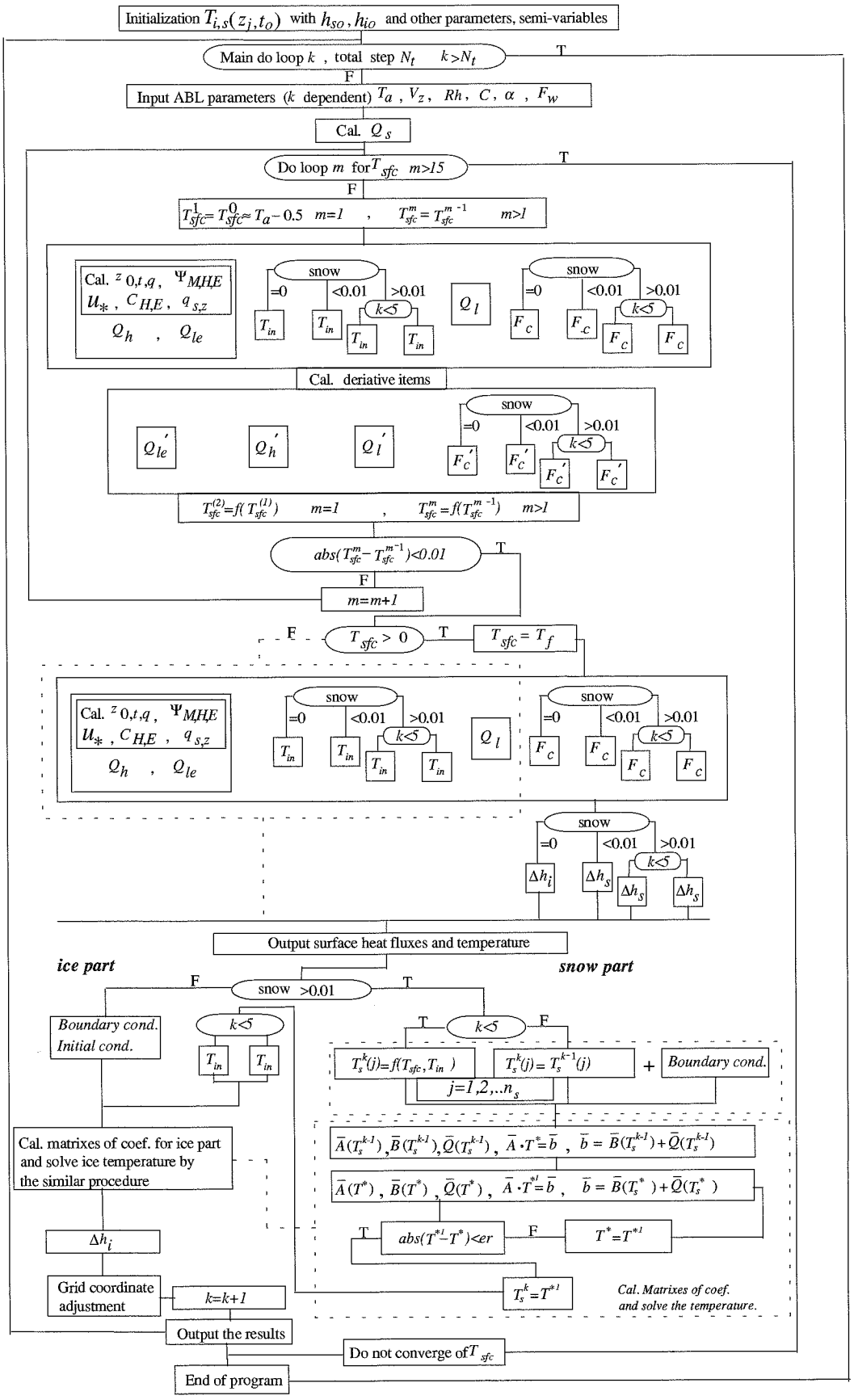

Fig. 6. Program flow diagram.

Short-wave radiation (subroutine: qsw.f)

$$Q_0 = S_0 \cos^2 Z \Big/ \left((\cos Z + 2.7)\cdot e \times 10^{-3} + 1.085\cdot \cos Z + 0.10\right)$$ *Zillman (1972)*

$$Q_0 = S_0 \cos^2 Z \Big/ \left((\cos Z + 1.0)\cdot e \times 10^{-3} + 1.2\cdot \cos Z + 0.0455\right)$$ *Shine (1984)*

$$\cos Z = \sin\phi \sin\delta + \cos\phi \cos\delta \cos HA$$

$$\delta = 23.44^\circ \cos[(172 - J)\pi / 180]$$

$$HA = (12 - h_t)\pi / 12$$

reduction in downwelling radiation due to cloudiness

$$Q_s = Q_0 \cdot (1 - 0.52 \cdot C)$$ *Bennett (1982)*

Long-wave radiation (subroutine: qlw.f)

$$Q_b = \varepsilon_0 \cdot \sigma \cdot T_{sfc}^4$$

Q_{d0} *as one of those below*

$$Q_{d0} = \left(1 - (1 + 46.5(e / T_a)) \cdot e^{-\sqrt{1.2 + 139.5\cdot(e/T_a)}}\right) \cdot \sigma \cdot T_a^4$$ *Prata (1996)*

$$Q_{d0} = (0.746 + 0.0066 \cdot e) \cdot \sigma \cdot T_a^4$$ *Efimova (1961)*

$$Q_{d0} = \sigma \cdot T_a^4 - 85.6$$ *Guest (1997)*

reduction in downwelling radiation due to cloudiness

$$Q_d = Q_{d0} \times (1 + 0.26 \cdot C)$$ *Jacobs (1978)*

Turbulent fluxes of sensible and latent heat (subroutine: coe.f)

(cf. Launiainen & Cheng, 1995)

$$Q_h = -\rho_a \cdot c_p \cdot C_H \cdot (T_{sfc} - T_z) \cdot V_z$$

$$Q_{le} = -\rho_a \cdot C_E \cdot (q_s - q_z) \cdot V_z \cdot R_l$$

$$\rho_a = 349 / T_a$$

$$R_l = (2500 - 2.375 \cdot (T_{sfc} - 273.15)) \times 1000.0 \qquad T_{sfc} \geq 273.15$$

$$R_l = (2500 - 2.375 \cdot (T_{sfc} - 273.15)) \times 1000.0 + 335 \times 10^3 \qquad T_{sfc} < 273.15$$

$$q_s = \frac{0.622 \cdot e_s}{P_0 - 0.378 \cdot e_s}$$

$$q_z = \frac{0.622 \cdot e}{P_0 - 0.378 \cdot e}$$

$$e_s = \varepsilon(T_{sfc})$$

$$C_D = \frac{{k_0}^2}{\left(\ln(z_a / z_0) - \Psi_M(\zeta)\right)^{-2}} = C_D\left(C_{DN}, \zeta\right)$$

$$C_H = \frac{{k_0}^2}{(\ln(z_a / z_0) - \Psi_M(\zeta))^{-1} \cdot (\ln(z_a / z_T) - \Psi_H(\zeta))^{-1}} = C_H\left(C_{HN}, \zeta\right)$$

$$C_E = \frac{{k_0}^2}{(\ln(z_a / z_0) - \Psi_M(\zeta))^{-1} \cdot (\ln(z_a / z_q) - \Psi_E(\zeta))^{-1}} = C_E\left(C_{EN}, \zeta\right)$$

z_0 , $z_{T,q}$ *over water surface*

$$C_{DN} = (0.61 + 0.063 \cdot V_z) \times 10^{-3}$$ *Smith (1980)*

$$C_{EN} = 0.63 \cdot C_{DN} + 0.32 \cdot 10^{-3}$$ *Launiainen (1983)*

$$\ln z_0 = \ln 10 - k_0 \cdot {C_{DN}}^{-1/2}$$

$$\ln z_T \approx \ln z_q = \ln 10 - k_0 \cdot {C_{DN}}^{1/2} \cdot {C_{EN}}^{-1}$$

z_0 , $z_{T,q}$ *over snow/ice surface*

$$C_{DN} = (1.10 + 0.072 \cdot \xi) \cdot 10^{-3}$$ *Banke & al. (1980)*

$$\ln z_0 = \ln 10 - k_0 \cdot {C_{DN}}^{-1/2}$$

$$\ln z_T \approx \ln z_q = \ln z_0 + b_0 + b_1 \cdot \ln(R_e) + b_2 \cdot \ln(R_e)^2$$ *Andreas (1987)*

$$R_e = z_0 \cdot u_* / \gamma = z_0 \cdot {C_{DN}}^{1/2} \cdot V_z / \gamma$$

$$\gamma = (0.9065 \cdot (T_z + 273.15) - 112.7) / 10^7$$

R_e	[0 0.135)	[0.135, 2.5)	[2.5, 1000]
b_0	1.43	0.25	0.356
b_1	0.0	-0.589	-0.538
b_2	0.0	0.0	-0.181

unstable stratification ($R_z < 0$),

$$\Psi_M = 2\ln\left(\frac{1+\Phi_M^{-1}}{2}\right) + \ln\left(\frac{1+\Phi_M^{-2}}{2}\right) - 2\overline{arc}\tan\Phi_M^{-1} + \frac{\pi}{2}$$ *Businger & al. (1971)*

$$\Psi_H = \Psi_E = 2\cdot\ln\left(\frac{1+\Phi_{H,E}^{-1}}{2}\right)$$ *Dyer (1974)*

$$\Phi_M = (1-19.3\cdot\zeta)^{-1/4}$$ *Högström (1988)*

$$\Phi_H = \Phi_E = (1-12.0\cdot\zeta)^{-1/2}$$

$$\zeta \equiv z_a / L \approx \left(\frac{(\ln z_a / z_0)^2}{(\ln z_a / z_T)} - 0.55\right)\cdot R_z$$ *Launiainen (1995)*

stable stratification ($R_z > 0$),

$\Psi_M \approx \Psi_{H,E} = -5\times 0.75/0.35 - 0.7\cdot\zeta - 0.75\cdot(\zeta - 5/0.35)\exp(-0.35\cdot\zeta)$ *Holtslag and De Bruin (1988)*

$\zeta \equiv z_a / L = (1.89\cdot\ln(z/z_0) + 44.2)R_z^2 + (1.18\ln(z/z_0)R_z - 1.5\ln(z_0/z_T) - 1.37)R_z$ *Launiainen (1995)*

$$R_z = \frac{z_a\cdot g\cdot(T_z - T_s)}{0.5\cdot(T_z + T_s)\cdot V_z^2}$$

ABL profile (subroutine: abl.f)

$$V(z_a) = \frac{u_*}{k_0}\left(\ln z_a/z_0 - \Psi_M(z_a/L)\right)$$

$$T(z_a) = T_s + \frac{Q_h}{\rho_a\cdot c_p k_0\cdot u_*}\left(\ln z_a/z_T - \Psi_H(z_a/L)\right)$$

$$q(z_a) = q_s + \frac{Q_{le}}{\rho_a\cdot k_0\cdot R_l\cdot u_*}\left(\ln z_a/z_q - \Psi_E(z_a/L)\right)$$

Penetrating solar radiation (subroutine: qin.f)

white ice *Grenfell & Maykut (1977)*

$\kappa = 17.1\cdot(1-C) + 10.5\cdot C$ $z \le 0.1$

$I = (1-\alpha)\cdot Q_s\cdot e^{-\kappa\cdot z}$

$\kappa = 1.5$ $z > 0.1$

$i_0 = 0.18\cdot(1-C) + 0.35\cdot C$

$I(z) = i_0\cdot(1-\alpha)\cdot Q_s\cdot e^{-\kappa\cdot(z-0.1)}$

blue ice *Grenfell & Maykut (1977)*

$$\kappa = 8.4 \cdot (1 - C) + 4.6 \cdot C \qquad z \le 0.1$$

$$I = (1 - \alpha) \cdot Q_s \cdot e^{-\kappa \cdot z}$$

$$\kappa = 1.4 \qquad z > 0.1$$

$$i_0 = 0.43 \cdot (1 - C) + 0.63 \cdot C$$

$$I(z) = (1 - \alpha) \cdot Q_s \cdot e^{-\kappa(z - 0.1)}$$

Conductive flux at the upper surface (subroutine: ts.f)

$$F_c = (k_i \frac{\partial T_i}{\partial z})_{sfc} = F_c(T_{sfc}) \approx k_i(T_i) \cdot \frac{T_i^1 - T_{sfc}}{\Delta h_i}$$

$$h_s \le 0.01m$$

$$F_c = (k_s \frac{\partial T_s}{\partial z})_{sfc} = F_c(T_{sfc}) \approx k_s \cdot \frac{T_{in} - T_{sfc}}{h_s}$$

$$k_s \cdot \frac{T_{in} - T_{sfc}}{h_s} = k_i \cdot \frac{T_i^1 - T_{in}}{\Delta h_i}$$

$$h_s > 0.01m$$

$$F_c = F_c(T_{sfc}) \approx k_s \cdot \frac{T_s^1 - T_{sfc}}{\Delta h_s}$$

$$\Delta h_s = h_s / n_s$$

$$\Delta h_i = h_i / n_i$$

Sea ice properties (subroutine: nume.f)

$$s_i = 4.6 + 0.916 / h_i$$ *Kovacs (1996)*

$$s_i = 14.2 - 19.4 h_i \qquad h_i < 0.6$$ *Cox & Weeks (1974)*

$$s_i = 3.0 \qquad h_i \ge 0.6$$

$$(\rho c)_s = \rho_s (92.88 + 7.364 \cdot T_s)$$ *Anderson (1976)*

$$k_s = 2.2236 (\rho_s)^{1.885}$$ *Yen (1981)*

$$(\rho c)_i = (\rho c)_{if} + 17.2 \times 10^6 \cdot s_i / (T_i - 273)^2$$ *Maykut & Untersteiner (1971)*

$$k_i = k_{if} + 0.117 \cdot s_i / (T_i - 273)$$

Phase change (subroutine: dhs.f)

surface:

$$(1-\alpha)Q_s(1-e^{-\kappa\cdot\Delta h})+Q_d-Q_b(T_f)+Q_h(T_f)+Q_{le}(T_f)+F_i(T_f)=-\rho_{i,s}L_{if,sf}\,dh_{i,s}/dt$$

$$h_{i,s}{}^{k}=h_{i,s}{}^{k-1}-\frac{\Delta t}{\rho_{s,i}\cdot L_{if,sf}}(1-\alpha)Q_s(1-e^{-\kappa\cdot\Delta h})+Q_d-Q_b(T_f)+Q_h(T_f)+Q_{le}(T_f)+F_i(T_f)$$

bottom:

$$-\rho_i\cdot L_{if}\cdot dh_i/dt=\left((-k_i\,\partial T_i/\partial z)_{bot}+F_w\right)$$

$$h_i^k=h_i^{k-1}-\frac{\Delta t}{\rho_i\cdot L_{if}}\left(\left(k_i\frac{T_b-T_i^{n_i-1}}{\Delta h}\right)-F_w\right)$$

total thickness change:

$$dh_i(t)\Big/dt=\left(h_i(t)^{k+1}-h_i(t)^k\right)\Big/\Delta t$$

Surface temperature (subroutine: ts.f)

Two alternatives for solving surface temperature

iterative

$$T_{sfc}^{k+1}=T_{sfc}^k-F(T_{sfc}^k)\Big/F'(T_{sfc}^k)$$

$$F'(T_{sfc})=-Q_b'(T_{sfc})+Q_h'(T_{sfc})+Q_{le}'(T_{sfc})+F_c'(T_{sfc})$$

approximate

$$(1-\alpha)Q_s(1-e^{-\kappa\cdot z_h})+Q_d-\varepsilon_0\cdot\sigma\cdot T_{sfc}^4+Q_h(T_{sfc})+Q_{le}(T_{sfc})+\frac{k_i}{\Delta h_i}\left(T_i^1-T_{sfc}\right)=0$$

$$T_{sfc}=T_p+\Delta T$$ *Semtner (1976)*

$$T_{sfc}^4=(T_p+\Delta T)^4\approx T_p^4+4T_p^3\Delta T$$

if $h_s=0$

$$\Delta T=\frac{(1-\alpha)Q_s(1-e^{-\kappa\cdot z})+Q_d-\varepsilon_0\cdot\sigma\cdot T_p^4+Q_h(T_p)+Q_{le}(T_p)+\frac{k_i}{\Delta h_i}\left(T_i^1-T_p\right)}{4\varepsilon_0\cdot\sigma\cdot T_p^3+\frac{k_i}{\Delta h_i}}$$

if $h_s\le 0.01m$

$$\Delta T = \frac{(1-\alpha)Q_s(1-e^{-\kappa\cdot z}) + Q_d - \varepsilon_0\cdot\sigma\cdot T_p^4 + Q_h(T_p) + Q_{le}(T_p) + \dfrac{k_s\cdot k_i}{k_s\Delta h_i + k_i h_s}\left(T_i^1 - T_p\right)}{4\varepsilon_0\cdot\sigma\cdot T_p^3 + \dfrac{k_s k_i}{k_s\Delta h_i + k_i h_s}}$$

if $h_s > 0.01m$

$$\Delta T = \frac{(1-\alpha)Q_s(1-e^{-\kappa\cdot z}) + Q_d - \varepsilon_0\cdot\sigma\cdot T_p^4 + Q_h(T_p) + Q_{le}(T_p) + \dfrac{k_s}{\Delta h_s}\left(T_s^{n_s-1} - T_p\right)}{4\varepsilon_0\cdot\sigma\cdot T_p^3 + \dfrac{k_s}{\Delta h_s}}$$

Normally, the quick approximate method gives results close to the iterated one. It is used e.g. when coupling the ice model with other models.

Snow/ice interface temperature T_{in} (subroutine: tint.f)

$$T_{in} = T_{sfc} \qquad h_s = 0$$

$$T_{in} = \frac{k_i h_s T_i^1 + k_s \Delta h_i T_s}{k_s\Delta h_i + k_i h_s} \qquad h_s \le 0.01m$$

$$T_{in} = \frac{k_i \Delta h_s T_i^1 + k_s \Delta h_i T_s^{n_s-1}}{k_s\Delta h_i + k_i \Delta h_s} \qquad h_s > 0.01m$$

VERIFICATION AND RUNNING OPERATIONS

The model was used to simulate ice growth in the Baltic Sea, and studies with respect to the Bohai Sea ice thermodynamics and theoretical examples of Antarctic sea ice were calculated. Two figures from those case studies are given below.

For specific case studies, the user can give a full set of parameters and semi-variables in input parameter files. An example is given in Table 1. Instructions for operation are given as specific notes in the program code.

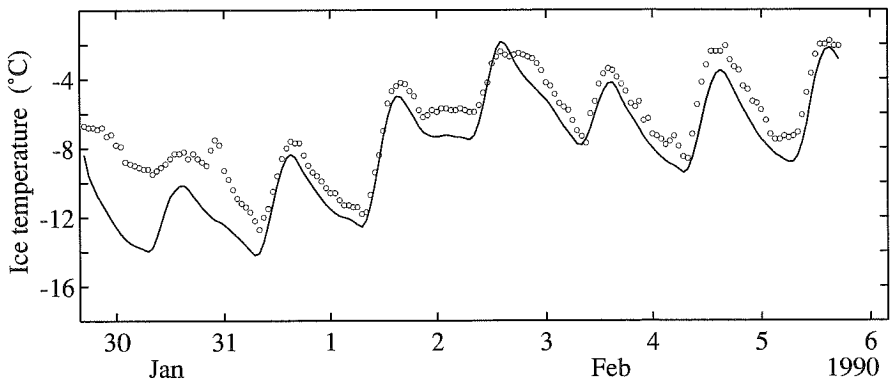

Fig. 7. In-ice temperature time series. The solid line gives the calculated temperature at a depth of 6 cm from the surface. Circles give the observed temperature. The field observation was carried out in the Bohai Sea (from Launiainen & Cheng, 1998).

Table 1. Coefficients and parameters for the model.

Name	Value
aerodynamic roughness, z_0	10^{-4} m
albedo, α_i , α_s	0.5 - 0.8 (ice), 0.80 (snow)
density of air, ρ_a	1.26 - 1.36 kg/m^3
density of ice, ρ_i	915 kg/m^3
density of snow, ρ_s	150 kg/m^3
extinction coefficient of ice, κ	1.5 - 17 m^{-1}
extinction coefficient of snow, κ	15 - 25 m^{-1}
freezing temperature, T_b	-1.8 °C
heat capacity of air, c_p	1004 J/kg K
heat capacity of ice, c_i	2093 J/kg K
latent heat of fusion of ice, L_{if}	0.33x10^6 J/kg
latent heat of fusion of snow, L_{sf}	0.054x10^6 J/kg
oceanic heat flux, F_w	2.0 - 5.0 W/m^2 (sometimes sign. larger)
thermal conductivity of ice, k_{if}	2.03 W/m K
thermal conductivity of snow, k_s	0.19 W/m K
Boltzmann constant, σ	5.68x10^{-8} W/m^2 K
solar constant, S	1367 W/m^2
von Karman constant k_0	0.405

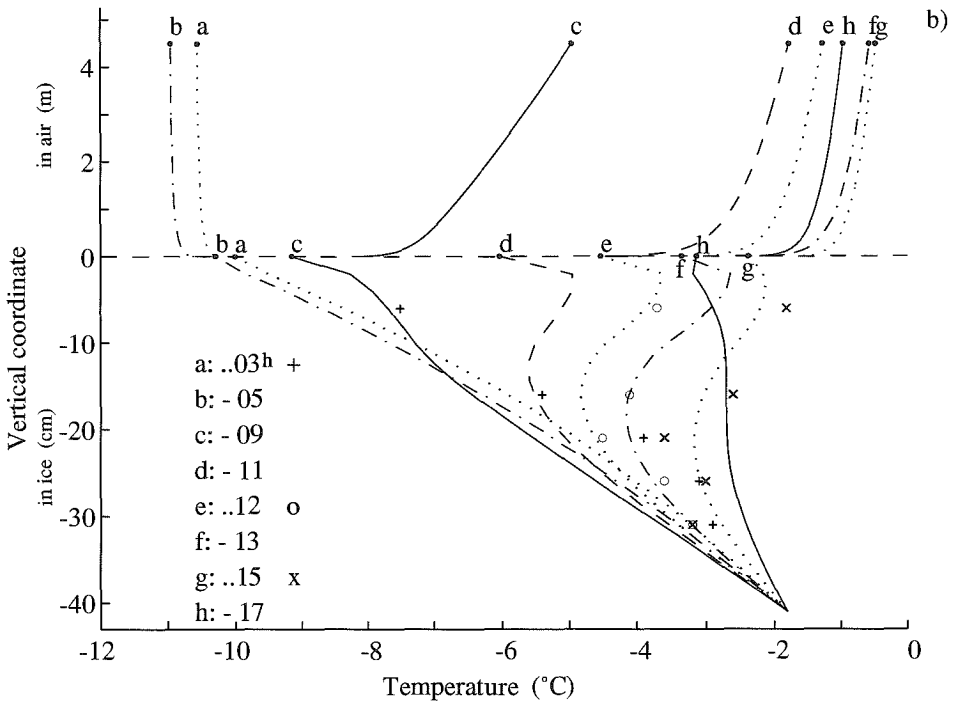

Fig. 8. Vertical air and in-ice temperature profiles during a single day (5 February 1990, from 03^h to 17^h). The few available observations are shown (+, o, x) for comparison. Note the different vertical scaling in ice and air (from Launiainen & Cheng, 1998).

CONCLUSION

A one-dimensional thermodynamic air-ice-sea model with all the parameterizations and coefficients, solution method of the model and algorithm and flow are introduced in this report. Each process is constructed as a single subroutine. The model code is written in Fortran, which allows the model to be easily coupled with other models.

ACKNOWLEDGEMENTS

Professor Matti Leppäranta and Mr. Zhanhai Zhang in the Department of Geophysics, University of Helsinki are thanked for their participation in discussions about sea ice thermodynamics and the numerical method. This work was financially supported by the Ministry of Trade and Industry of Finland. Finally, realisation of the project "Baltic Air-Sea-Ice Study", funded by EU contract MAS3-CT97-0117, favourably assisted the practical development and generalization of the model, as a module capable of integration with other case studies and models.

REFERENCES

Anderson, E.A. 1976. A point energy and mass balance model of a snow cover. - NOAA Tech. Rep. NWS 19, Natl. Oceanic and Atmos. Admin., Washington, D.C.

Andreas, E.L. 1987. A theory for the scalar roughness and the scalar transfer coefficients over snow and sea ice. - Boundary-Layer Meteorol. 38:159-184.

Banke, E.G., Smith, S.D. & Anderson, R.J. 1980. Drag coefficient at AIDJEX from sonic anemometer measurement. - In: Pritchard, R.S. (ed.), Sea Ice Processes and Models. University of Washington Press, Seattle, pp. 430-442.

Bennet, T.J. 1982. a coupled atmosphere-sea-ice model study of the role of sea-ice in climatic predictability. - J. Atmos. Sci. 39: 1456-1465.

Businger, J.A., Wyngaard, J.C., Izumi, Y. & Bradley, E.F. 1971. Flux-profile relationships. - J. Atmos. Sci. 28: 181-189.

Cheng, B., 1996. The conservative difference scheme and numerical simulation of one dimensional thermodynamic sea ice model. - M. Sci. Bull., 15(4): 8-15 (in Chinese).

Cox, G.F.N. & Weeks, W.F. 1974. Salinity variations in sea ice. - J. Glaciol. 13: 109-120.

Dyer, A.J. 1974. A review of flux-profile relationship. - Boundary-Layer Meteorol. 7: 363-372.

Efimova, N.A. 1961. On methods of calculating monthly values of net long-wave radiation. - Meteorol. Gidrol., 10: 28-33.

Grenfell, T.C. & Maykut, G.A. 1977. The optical properties of ice and snow in the Arctic Basin. - J. Glaciol. 18: 445-463.

Guest, P.P. 1997. Surface radiation conditions in the Eastern Weddell Sea during winter. (Manuscript)

Holtslag, A.A.M. & De Bruin, H.A.R. 1988. Applied modeling of the nighttime surface energy balance over land. - J. Appl. Meteorol. 37: 689-704.

Högström, U. 1988. Non-dimensional wind and temperature profiles in the atmospheric surface layer: A re-evaluation. - Boundary-Layer Meteorol. 42: 55-78.

Iribarne, J.V. & Godson, W.L. 1973. Atmospheric thermodynamics. - D. Reidel Publishing Company, 222 pp.

Jacobs, J.D. 1978. Radiation climate of Broughton Island. - In: Barry, R.G. and Jacobs, J.D. (eds), Energy budget studies in relation to fast-ice breakup psocesses in Davis Strait. - Occas. Pap. 26: 105-120. Inst. of Arctic and Alp. Res., Univ. of Colorado, Boulder.

Kovacs, A. 1996. Sea ice, Part I. Bulk salinity versus ice floe thickness. - CRREL Report No. 7.

Launiainen, J. 1983. Parameterization of the water vapour flux over a water surface by the bulk aerodynamic method. - Annales Geophysicae, 1: 481-492.

Launiainen, J. 1995. Derivation of the relationship between the Obukhov stability parameter and the bulk Richardson number for the flux-profile studies. - Boundary-Layer Meteorol., 76: 165-179.

Launiainen, J. & Cheng, B. 1995. A simple non-iterative algorithm for calculating turbulent bulk fluxes in diabatic conditions over water, snow/ice and ground surface. - Report Series in Geophysics, 33. Dept. of Geophysics, University of Helsinki.

Launiainen, J. & Cheng, B. 1998. Modelling of ice thermodynamics in natural water bodies. - Cold Reg. Sci. Technol., 27: 153-178.

Maykut, G.A. & Untersteiner, N. 1971. Some results from a time dependent thermodynamic model of sea ice. - J. Geophys. Res. 76(6): 1550-1575.

Prata, A.J. 1996. A new long-wave formula for estimating downward clear-sky radiation at the surface. - Q.J.R. Meteorol. Soc., 122: 1127-1151.

Semtner, A.J. 1976. A model for the thermodynamic growth of sea ice in numerical investigaiton of climate. - J. Phys. Oceanogr. 6: 379-389.

Shine, K.P. 1984. Parameterization of short wave flux over high albedo surfaces as a function of cloud thickness and surface albedo. - Q.J.R. Meteorol. Soc., 110: 747-764.

Smith, S.D. 1980. Wind stress and heat flux over the ocean in gale force winds. - J. Phys. Oceanogr. 10: 709-726.

Yen, Y.-C. 1981. Review of thermal properties of snow, ice and sea ice. - CRREL Report No 10.

Zillman, J.W. 1972. A study of some aspects of the radiation and heat budgets of the southern hemisphere oceans. - Meteorol. Stud. Rep. 26, Bur. of Meteorol., Dept. of the Inter., Canberra, A.C.T.

List of symbols

C	cloud factor (0 to 1.0)
$C_{D,H,E}$	bulk transfer coefficients in diabatic conditions
C_{DN}	turbulent bulk transfer coefficient for momentum under neutral stratification
C_{EN}	turbulent bulk transfer coefficient for latent heat (Dalton number) under neutral stratification
C_{HN}	turbulent bulk transfer coefficient for sensible heat (Stanton number) under neutral stratification
C_{HW}	heat exchange coefficient between water and ice
F_c	conductive heat flux near the surface (W/m^2)
F_m	heat flux due to melting of ice or snow (W/m^2)
F_Q	surface heat fluxes non-dependent on the surface temperature (W/m^2)
$F_Q(T_{sfc})$	surface heat fluxes dependent on the surface temperature (W/m^2)
F_w	heat flux from water below (W/m^2)
HA	hour angle
$I(z,t)$	penetrating solar radiation (W/m^2)
J	Julian day
L	Monin-Obukhov length (m)
L_{if}	heat of fusion of saline ice (J/kg)
L_{sf}	heat of fusion of snow (J/kg)
P_0	standard air pressure at the surface (hPa)
Q_0	solar radiation in clear sky conditions (W/m^2)
Q_b	emitted long-wave radiation (W/m^2)
Q_c	heat conduction in snow and ice (W/m^2)
Q_d	downwelling long-wave radiation (W/m^2)
Q_{d0}	incoming atmospheric long-wave radiation under clear sky conditions (W/m^2)

Q_h	sensible heat flux (W/m^2)
Q_l	net long-wave radiation (W/m^2)
Q_{le}	latent heat flux (W/m^2)
Q_s	downward short-wave radiation (W/m^2)
Rh	relative humidity (%)
R_e	Reynolds number
R_l	enthalpy of vaporization (Ws/kg)
R_z	bulk Richardson number
S_0	solar constant (W/m^2)
T_a	air temperature (K)
T_b	ice bottom temperature (K)
T_{dew}	dew point temperature (K)
T_{dry}	dry-bulb temperature (K)
T_f	freezing point (K)
T_i	ice temperature (K)
T_{in}	snow-ice interface temperature (K)
T_{iso}	initial snow and ice temperature (K)
T_p	temperature at the previous time step (K)
T_{sfc}	surface temperature (K)
T_s	snow temperature (K)
T_w	water temperature (K)
T_{wet}	wet-bulb temperature (K)
T_z	air temperature at height z (K)
T_0	mean temperature (K)
V_z	wind speed at height z (m/s)
W	current velocity (m/s)
Z	solar zenith angle
c_{if}	heat capacity of ice (J/kg K)
c_p	specific heat of air (Ws/kg K)
c_w	specific heat of water (J/kg K)
e	vapour pressure (hPa)
g	acceleration due to gravity (m/s^2)
h_i	thickness of ice (m)
h_{io}	initial thickness of ice (m)
h_s	thickness of snow (m)
h_{so}	initial thickness of snow (m)
h_t	solar time (hour)

k_0	von Karman constant
k_i	thermal conductivity of sea ice (W/m K)
k_{if}	thermal conductivity of fresh water ice (W/m K)
k_s	thermal conductivity of snow (W/m K)
n_i	number of nodal of subdivisions in ice
n_s	number of nodal of subdivisions in snow
$q(z,t)$	internal heat source or sink in the ice or snow (W/m^2)
q_s	specific humidity at the surface
q_z	specific humidity at height z
φ	scaling humidity
s_i	sea ice salinity (ppt)
t	time (s)
u_*	friction velocity (m/s)
z	vertical coordinate in the snow and ice (m)
z_0	roughness length for wind speed (m)
z_a	vertical height above the surface (m)
z_q	roughness length for water vapour (m)
z_t	roughness length for temperature (m)
α_i	ice albedo
τ	snow albedo
δ	declination of the sun
ε_0	surface emissivity
ε	saturation pressure of water vapour (hPa)
φ	latitude
γ	kinematic viscosity of air (m^2/s)
κ_i	extinction coefficient in ice (m^{-1})
κ_s	extinction coefficient in snow ($m^{-1)}$
θ	adjustment parameter for the numerical scheme
θ_*	scaling temperature
ρ_a	density of air (kg/m^3)
ρ_i	density of sea ice (kg/m^3)
ρ_s	density of snow (kg/m^3)
ρ_w	density of water (kg/m^3)
σ	Boltzman constant ($W/m^2\ K^4$)
τ	turbulent flux of momentum (N/m^2)
ξ	geometric surface roughness (cm)
ζ	Monin-Obukhov stability parameter
Δh_i	thickness of each layer of ice (m)

Δh_s	thickness of each layer of snow (m)
Δt	time step (s)
ΔT	perturbation of surface temperature (°C)
Φ_M	gradient universal function for momentum
Φ_H	gradient universal function for heat
Φ_E	gradient universal function for moisture
Ψ_M	integrated universal function for momentum
Ψ_H	integrated universal function for heat
Ψ_E	integrated universal function for moisture

Subscripts

i	refers to ice
s	refers to snow
w	refers to water
N	refers to dimension of matrix
j	refers to spatial development
bot	refers to bottom
sfc	refers to surface

Superscript

'	refers to derivative
k	refers to time development
—	refers to matrix

LITERATURE REVIEW ON MICROBIOLOGY OF AGGREGATES ORIGINATING FROM PHYTOPLANKTON BLOOMS

Susanna Hietanen

Finnish Institute of Marine Research, P.O. Box, 33, 00931, Helsinki, Finland

1. INTRODUCTION

Formation of visible, macroscopic aggregates of microscopic particles in the water is a common phenomenon in oceans, lakes and rivers (Alldredge & Silver 1988, Weiss & al. 1996, Zimmermann & Kausch 1996, Zimmermann 1997, Grossart & al. 1998). These aggregates are often called "marine snow" or "lake snow". This quite descriptive term was introduced as early as in the 1950s by Suzuki & Kato (1953) after Carson (1951) described sedimenting material reaching the see floor as a "long snowfall". Since then the aggregates have been studied intensively.

The ecological importance of marine snow lies in the special nature of aggregates when compared to microscopic particles. Aggregated material sinks faster than individual particles. Therefore aggregation removes carbon and nutrients from the productive surface layer (Fowler & Knauer 1986). Aggregation of bacteria and algae into bigger flocs also changes the grazing chain to favour large-particle feeders (e.g. crustaceans) at the expense of the microbial loop grazers (e.g. protozoa) (Alldredge & Silver 1988). In addition the optical properties of water are affected when particles stick together since it alters the size distribution and abundance of particles available to absorb and scatter light (Alldredge & Jackson 1995). Aggregates are known to form special enriched patches of carbon and nutrients as well as support distinct food webs of microbes and protozoa (e.g. Shanks & Trent 1979, Caron & al. 1986, Fowler & Knauer 1986, Alldredge & Cohen 1987, Alldredge & Silver 1988, Gotschalk & Alldredge 1989, Riebesell 1991b, Kaltenböck & Herndl 1992). Recently many studies have focused on anoxic microniches formed inside aggregates as a result of microbial degradation of organic matter (Paerl 1985, Paerl & Prufert 1987, Bianchi & al. 1992, Shanks & Reeder 1993, Ploug 1997).

2. FORMATION, BREAKDOWN AND LOSS OF AGGREGATES

Particulate matter in surface waters consists of living organisms, inorganic particles and detritus. Aggregation of these is a complex process involving both physical, chemical and biological interactions between particles.

Physical processes such as shear (differences in fluid movements bring particles together), Brownian motion (thermal movement of one particle towards another) and differential settlement (one particle sinks faster than the other, overtaking and colliding with it) bring particles together in the water column (Jackson 1994). Chemical and biological properties of colliding particles ("stickiness") determine whether they stay together. The mucus sheaths as well as other organic surface materials, especially polysaccharide particles known as transparent exopolymer particles (TEP) around the organisms, act as adsorption surfaces for other particles (Alldredge & Silver 1988, Alldredge & al. 1993, Passow & al. 1994). Attachment to surfaces has been proved to stimulate bacterial exopolysaccharide synthesis, further enhancing aggregation (Vandevivere & Kirchman 1993). The microaggregates formed collide with each other forming macroaggregates, visible "marine snow".

Aggregate size can also decrease because of physical and biological processes. Turbulence tears particles physically apart as well as brings them together (McCave 1984, Riebesell 1991a). Biological disaggregation, including consumption by zooplankton or nekton and decomposition by microorganisms, can on some occasions be a more important factor regulating aggregate size than abiotic fragmentation (Taylor & al. 1986, Alldredge & al. 1990).

Aggregates are lost from the upper water layer by sedimentation, which is enhanced by growing aggregate size, and by grazing (Alldredge & Silver 1988). Grazing of aggregates by fish and zooplankton has recently been proved to be an important shortcut in the food chain, transferring organic carbon to higher trophic levels more efficiently than via the microbial loop (Lampitt & al. 1993, Grossart & al. 1998). The relative importance of these mechanisms in aggregate disappearance depends on the origin and age of the aggregates (Biddanda & Pomeroy 1988, Riebesell 1991a, Turley 1992).

2.1 Aggregation and fate of diatom bloom

A two-state coagulation theory, in which coagulation is insignificant at low and significant at high algal concentrations with a rapid transition between these two states, seems to adequately describe the dynamics of diatom blooms (Jackson 1990, Riebesell 1991a, Kiørboe & al. 1994). At the beginning of the bloom there is no coagulation of cells into aggregates neither is there any sinking of cells out of the euphotic zone. The concentration of diatom cells increases rapidly until a critical limit is reached. The critical cell concentration depends on cell sizes, cell surface "stickiness" and turbulence of water. At the critical concentration the cells aggregate, sometimes extremely quickly - the whole bloom aggregated and sedimented in 24 hours in the study of Alldredge & Gotschalk (1989). This pattern for diatom bloom dynamics has also been reported from the Baltic Sea spring bloom - an initial intensive bloom followed by rapid sedimentation as a result of nutrient depletion (Leppänen 1988, Leppänen & Kononen 1988, Kuparinen & al. 1996, Kankaanpää & al. 1997). Nutrient depletion at the end of a bloom has been shown to increase diatom cell stickiness, enhancing aggregation (Smetacek 1985, Logan & Alldredge 1989, Kiørboe & al. 1994). Even if the algal cells keep dividing, the particle concentration does not increase further since new production aggregates quickly (Jackson 1990, Riebesell 1991b). Aggregates are colonised by bacteria and protozoa (Alldredge & Gotschalk 1990, Simon & al. 1990, Zimmermann & Kausch 1996), but because of the relatively high density of diatom aggregates they sink rapidly from the productive layer before major decomposition takes place (Smetacek 1985, Alldredge & Gotschalk 1989, Riebesell 1991b).

2.2 Aggregation and fate of cyanobacteria bloom

Cyanobacterial blooms also aggregate, especially as they age (Hoppe 1981), but the fate of cyanobacterial aggregates differs from that of diatom aggregates. Intracellular gas vacuoles prevent sedimentation, keeping aggregated filaments in the upper water layer (Hoppe 1981, Worm & Søndergaard 1998). Grazing losses are also insignificant since grazers avoid cyanobacteria because of their "difficult" size and shape (filaments, colonies and especially aggregates) and potential toxicity (e.g. Estep & Vigg 1985, Haney 1987). As a result, cyanobacterial aggregates are soon colonised by bacteria and protozoa, becoming sites of enhanced biological, especially microbial, activity (Paerl 1976, Caldwell & Caldwell 1978, Silver & al. 1978, Hoppe 1981, Caron & al. 1982, Zimmermann & Kausch 1996, Grossart & al. 1998). These conditions can predominate for weeks, even months (Hoppe 1981), until increased turbulence disaggregates the whole bloom (Heiskanen & Kononen 1994).

3. ABUNDANCE OF AGGREGATES

Abundance of aggregates cannot be estimated by traditional water sampling methods because of the extreme fragility of the flocs. Therefore a variety of advanced methods, each of which has some drawbacks, have been developed to study aggregate quantities.

Traditional sediment traps seem to either destroy aggregates if preservatives (e.g. formalin) are used or, in the absence of such agents, lose some matter by biodegradation. Large volume *in situ* filtration systems (LVFS) provide data on particle numbers and size distribution in the water column, also allowing particle density calculations. It still remains unclear, however, what these deep-sea pumps actually sample ("suspended particles" v. "large, fast sinking particles"). Most studies rely on laborous hand collection *in situ* by SCUBA diving, some take advantage of submersibles. Recent advances in *in situ*

photography and video techniques have made these methods useful in aggregate as well as other marine studies (reviewed by Fowler & Knauer 1986).

Table 1. Abundance of aggregates at some locations.

Location	Abundance, l^{-1}	Method	Reference
Subtropical Atlantic, Bahama Islands	0.0005-0.004	Submersible	Alldredge & Youngbluth 1985
Gulf Stream	0.1	SCUBA / hand collection	Alldredge & al. 1986
Californian coast	4.3	SCUBA / hand collection	Alldredge & al. 1986
Californian coast	0.5-12.9	SCUBA / hand collection	Alldredge & Gotschalk 1989
Californian coast	0.2-1.65	SCUBA / hand collection	Alldredge & Gotschalk 1990
Californian coast	0.2-1.65	SCUBA / number of aggr. passing through a hand-held loop in a given distance	Simon & al. 1990
German Bight	425-5300	Underwater camera	Riebesell 1991a
Antarctic coast	0.1-10	Remote-controlled video camera	Marchant & al. 1996
Lake Constance, Germany	5-20	SCUBA / hand collection	Weiss & al. 1996
Elbe Estuary	40-120	wide-mouth bottles	Zimmermann & Kausch 1996

4. MICROBIAL COLONISATION AND SUCCESSION IN AGGREGATES

Young and healthy phytoplankton cells seldom show any bacterial colonisation (Paerl 1976, Hoppe 1981). As the cells age, however, they start aggregating and quickly become attached by micro-organisms. The predominant sites for bacterial colonisation are the inactive cells along the filaments, preferably surrounded by mucilage (Caldwell & Caldwell 1978, Hoppe 1981, Grossart & al. 1998), and polar regions of heterocysts in cyanobacterial colonies, capable of nitrogen fixation (Paerl 1976). The bacterial population serves as a food source for e.g. protozoa, supporting a complex microecosystem (Silver & al. 1978, Hoppe 1981, Biddanda 1985, Taylor & al. 1986, Alldredge & Silver 1988, Alldredge & Gotschalk 1990, Zimmermann & Kausch 1996). Heterotrophic production blooms as long as primary production by phytoplankton cells supplies the heterotrophic community with the organic substrate it needs. In aging aggregates, senescent algae alone alone provide a sufficient amount of degradable material for the maintenance of a high standing stock of attached bacteria. Therefore the role of the "recycling" of organic matter from microzooplankton (as excretion, dead cells, fecal pellets, sloppy feeding) towards bacteria is emphasised as the aggregates get older (Hoppe 1981, Taylor & al. 1986, Biddanda & Pomeroy 1988). Cyanobacterial aggregates that avoid sedimentation and therefore stay in the upper water layer for weeks can reach a steady state in which the input and output of organic matter is balanced (Hoppe 1981). Müller-Niklas & al. (1994) showed that aging processes are, however, similar in buoyant and sinking particles. With increasing size and age, aggregates become poor habitats for bacterial growth. Rapid successional changes in microbial populations suggest that any labile matter available in newly formed aggregates is quickly utilised by bacteria (Alldredge & Silver 1988, Alldredge & Gotschalk 1990).

5. PROCESSES IN AGGREGATES

5.1 Primary production

The amount of primary production in aggregates depends e.g. on the size of the aggregate (shading in big aggregates, enhanced sinking), physical state of the algae in aggregate (healthy v. senescent cells),

availability of nutrients (nutrient recycling by attached bacteria, nitrogen fixation) and turbulence (keeping the cells in the productive water layer or allowing them sink). Therefore aggregation can either enhance or diminish the primary production of phytoplankton cells. As a general rule, the contribution of primary production in aggregates to the total primary production in the euphotic layer is significant only in newly formed, phytoplankton-originated aggregates (Alldredge & Gotschalk 1990).

5.2 Heterotrophic production

Abundance and heterotrophic production of attached bacteria has already been studied intensively for a couple of decades, but the results are still somewhat contradictory. Depending on the method used, location and time of year, the abundance and production of bacteria in aggregates has been claimed to be either significant or negligible compared to that of free-living bacteria (Table 2). This might also reflect discrepancies in the timing of sampling since microbial activity on marine snow is highly variable and depends on aggregate origin as well as aggregate age (Alldredge & Silver 1988, Herndl 1988, Alldredge & Gotschalk 1990).

Table 2. The abundance and production of attached bacteria compared to that of total pelagic bacteria at some locations.

Location	Attached bacteria, % of all	Method	Prod. of attached bacteria, ng C l^{-1} h^{-1}	% of total	Reference
Bilbao Coast, Spain	1-22				Iriberri & al. 1987
Elbe Estuary	75				Zimmermann 1997
Freshwater pond	<10	^{3}H-thymidine incorporation	1-10		Kirchman 1983
Subtropical Atlantic, Bahama Islands	<0.05	^{3}H-thymidine incorporation	0.00045-0.071	0.001-0.54	Alldredge & Youngbluth 1985
Adriatic Sea	20-30	^{3}H-thymidine incorporation	410-930	54 - 85	Karner & Herndl 1992
Lake Frediksborg Slossø, Denmark	8-32	^{3}H-thymidine incorporation	250-3770	25-43	Worm & Søndergaard 1998
Gulf Stream	0.1-4.4	^{3}H-thymidine incorporation		0.1-1.4	Alldredge & al. 1986
Californian coast	0.9-3	^{3}H-thymidine incorporation		0.2-2.8	Alldredge & al. 1986
Californian coast	0-2.2	^{3}H-thymidine incorporation	0.05-2.0	0.2-10.9	Alldredge & Gotschalk 1990
Californian coast		^{14}C-leucine incorporation	3-30	1-1.25	Simon & al. 1990
Lake Kinneret, Israel	25	^{14}C-leucine incorporation	1.4-3.5	0.26-0.37	Grossart & al. 1998

Many studies show that, on a cellular basis, attached bacteria are metabolically more active than free-living ones (Harvey & Young 1980, Kirchman & Mitchell 1982, Alldredge & Youngbluth 1985, Iriberri & al. 1987, Hoppe & al. 1988, Alldredge & Gotschalk 1990, Karner & Herndl 1992, Smith & al. 1992, Grossart & al. 1998, Worm & Søndergaard 1998). Others prove just the opposite: bacteria attached to marine snow do not grow any faster than free-living bacteria (Alldredge & al. 1986, Alldredge & Gotschalk 1990, Simon & al. 1990).

Generally, attached bacteria have been reported to be bigger than their free-living counterparts (Kirchman 1983, Alldredge & Youngbluth 1985, Alldredge & al. 1986, Iriberri & al. 1987, Herndl 1988, Alldredge & Gotschalk 1990, Smith & al. 1992, Zimmermann & Kausch 1996, Worm & Søndergaard 1998) but not always (Karner & Herndl 1992, Müller-Niklas & al. 1994).

It has recently been shown (by the use of modern gene technology) that distinct bacterial populations, totally different from free-living populations, develop in aggregates (DeLong & al. 1993, Weiss & al.

1996). This finding might explain some differences observed between free-living and attached bacteria since all bacterial groups found on aggregates in these studies are known to have special properties that make them well-adjusted to attached life (DeLong & al. 1993, Weiss & al. 1996). These special features include a tendency to associate and glide on surfaces as well as an ability to produce different exoenzymes and to degrade a variety of high molecular weight compounds (DeLong & al. 1993).

5.3 Nitrogen processes

Aggregates are known to be sites of intense nutrient cycling (e.g. Shanks & Trent 1979, Caron & al. 1986, Fowler & Knauer 1986, Alldredge & Cohen 1987, Alldredge & Silver 1988, Gotschalk & Alldredge 1989, Alldredge & Gotschalk 1990, Riebesell 1991b, Kaltenböck & Herndl 1992). This review only discusses nitrogen processes in cyanobacterial aggregates.

The biological nitrogen cycle consists of reactions that are mainly carried out by bacteria. Plants can assimilate ammonia and nitrate, but nitrogen fixation, ammonification, nitrification and denitrification are strictly microbial processes (Stanier & al. 1971). Likewise, anaerobic ammonium oxidation to dinitrogen gas has been shown to be a microbially mediated process (van de Graaf & al. 1995).

Cyanobacteria capable of fixing dissolved molecular nitrogen (N_2) regularly aggregate during intensive blooms. Since the sedimentation and grazing of these aggregates is minor (Hoppe 1981, Heiskanen & Kononen 1994), they have been considered a net nitrogen input in the ecosystem. Nevertheless, the fate of nitrogen fixed by cyanobacteria still remains uncertain. The alternatives in theory are that fixed nitrogen is released into the surrounding water as the cyanobacterial cells lyse at the end of the bloom (Heiskanen & Kononen 1994), or that nitrogen is at least partly converted back into gaseous dinitrogen by anaerobic denitrification processes.

Both nitrogen fixation and denitrification are oxygen-sensitive processes. Denitrifying bacteria are facultative anaerobes that denitrify in anaerobic environments, although some bacteria may simultaneously nitrify and denitrify in aerobic environments (Robertson & Kuenen 1984). Therefore, the formation of microscale anoxic patches in aggregates plays a key role in both nitrogen fixation and denitrification rates in aggregates. Anoxic microzones and denitrification have been demonstrated in activated sludge flocs at waste water treatment plants (de Beer & al. 1997). Recently, Michotey & Bonin (1997) demonstrated particle-associated denitrification in the Mediterranean Sea. Nitrogen fixation has been shown to be more active in cyanobacterial aggregates than in suspended filaments (Paerl 1985, Paerl & Prufert 1987). The existence of microniches in cyanobacterial aggregates has also been proved experimentally in many studies (Paerl 1985, Alldredge & Cohen 1987, Paerl & Prufert 1987, Bianchi & al. 1992, Shanks & Reeder 1993, Ploug & al. 1997), but the factors regulating their quantity are not totally understood. Aggregates, like sediments, provide both a colonisable surface and a concentrated source of readily metabolisable organic matter. Microbial degradation of organic matter results in oxygen-poor microzones around and inside particles (Paerl & Prufert 1987). Anoxic patches remain even in well-oxygenated surroundings as the physical structure provided by the aggregate slows down the diffusion in and out of the microzone (Shanks & Reeder 1993). Paerl (1985) and Ploug & al. (1997) point to the importance of low environmental turbulence and de Beer & al. (1997) to the complicated structure of aggregates in microzone formation. These requirements are easily met in cyanobacterial aggregates that form under almost non-existent turbulence and seem to actively fix both carbon and nitrogen.

6. SUMMARY

Phytoplankton-derived aggregates seem to be an important phenomenon in pelagic ecosystems, albeit ephemeral in an annual time scale.

Regular aggregation of phytoplankton blooms provides unique microenvironments with highly specialized populations and trophic interactions, thus increasing the biodiversity of oligotrophic pelagial waters.

Physical aspects of aggregation, disaggregation and aggregate loss from the water column seem to be quite well described. Our understanding of biological processes in aggregates however remains incomplete.

In order to estimate the contribution of aggregate-associated processes to those of free-living organisms, we need to focus on developing methods to measure the key processes in aggregates. The high metabolical rates detected so far in aggregates indicate that their role in the water column might be far greater than expected from their brief appearances.

REFERENCES

Alldredge, A.L. & Cohen, Y. 1987: Can microscale chemical patches persist in the sea? Microelectrode study of marine snow and fecal pellets. - Science 235: 689-691.

Alldredge, A., Cole, J.J. & Caron, D.A. 1986: Production of heterotrophic bacteria inhabiting macroscopic organic aggregates (marine snow) from surface waters. - Limnol. Oceanogr. 31: 68-78.

Alldredge, A.L. & Gotschalk, C.C. 1989: Direct observations of the mass flocculation of diatom blooms: characteristics, settling velocities and formation of diatom aggregates. - Deep-Sea. Res. 36: 159-171.

Alldredge, A.L. & Gotschalk, C.C. 1990: The relative contribution of marine snow of different origins to biological processes in coastal waters. - Cont. Shelf Res. 10: 41-58.

Alldredge, A.L., Granata, T.C., Gotschalk, C.C. & Dickey, T.D. 1990: The physical strength of marine snow and its implications for particle disaggregation in the ocean. - Limnol. Oceanogr. 35: 1415-1428.

Alldredge, A.L. & Jackson, G.A. 1995: Aggregation in marine systems. - Deep-Sea Res. 42: 1-7.

Alldredge, A.L., Passow, U. & Logan, B.E. 1993: The abundance and significance of a class of large, transparent organic particles in the ocean. - Deep-Sea Res. II. 40, 1131-1140.

Alldredge, A.L. & Silver, M.W. 1988: Characteristics, dynamics and significance of marine snow. - Prog. Oceanog. 20: 41-82.

Alldredge, A.L. & Youngbluth, M.J. 1985: The significance of macroscopic aggregates (marine snow) as sites for heterotrophic bacterial production in the mesopelagic zone of the subtropical Atlantic. - Deep-Sea Res. 32: 1445-1456.

de Beer, D., Schramm, A., Santegoeds, C.M. & Nielsen, H.K. 1997: Anaerobic processes in activated sludge. - Proceedings of Second International Conference on Microorganisms in activated sludge and biofilm processes: 783-786.

Bianchi, M., Marty, D., Teyssié, J.-L. & Fowler, S.W. 1992: Strictly aerobic and anaerobic bacteria associated with sinking particulate matter and zooplankton fecal pellets. - Mar. Ecol. Prog. Ser. 88: 55-60.

Biddanda, B.A. 1985: Microbial synthesis of macroparticulate matter. - Mar. Ecol. Prog. Ser. 20: 241-251.

Biddanda, B.A. & Pomeroy, L.R. 1988: Microbial aggregation and degradation of phytoplankton-derived detritus in seawater. I. Microbial succession. - Mar. Ecol. Prog. Ser. 42: 79-88.

Caldwell, D.E. & Caldwell, S.J. 1978: A *Zoogloea* sp. associated with blooms of *Anabaena flos-aquae*. - Can. J. Microbiol. 24: 922-931.

Caron, D.A., Davis, G.D., Madin, L.P. & Sieburth, J. McN. 1982: Heterotrophic bacteria and bacterivorous protozoa in oceanic macroaggregates. - Science 218: 795-797.

Caron, D.A., Davis, G.D., Madin, L.P. & Sieburth, J. McN. 1986: Enrichment of microbial populations in macroaggregates (marine snow) from surface waters of the North Atlantic. - J. Mar. Res. 44: 543-565.

Carson, R. 1951: The Sea Around Us. - Oxford University Press, 230 pp.

DeLong, E.F. , Franks, D.G. & Alldredge, A.L. 1993: Phylogenetic diversity of aggregate-attached vs. free-living marine bacterial assemblages. - Limnol. Oceanogr. 38: 924-934.

Estep, M.L.F. & Vigg, S. 1985: Stable carbon and nitrogen isotope tracers of trophic dynamics in natural populations and fisheries of the Lahontan Lake System, Nevada. - Can. J. Fish. Aquat. Sci. 42: 1712-1719.

Fowler, S.W. & Knauer, G.A. 1986: Role of large particles in the transport of elements and organic compounds through the oceanic water column. - Prog. Oceanog. 16: 147-194.

Gotschalk, C.C. & Alldredge, A.L. 1989: Enhanced primary production and nutrient regeneration within aggregated marine diatoms. - Mar. Biol. 103: 119-129.

Grossart, H-P., Berman, T., Simon, M. & Pohlmann, K. 1998: Occurrence and microbial dynamics of macroscopic organic aggregates (lake snow) in Lake Kinneret, Israel, in fall. - Aquat. Microb. Ecol. 14: 59-67.

Haney, J.F. 1987: Field studies of zooplankton - cyanobacteria interactions. - NZ J. Mar. Freshw. Res. 21: 467-475.

Harvey, R.W. & Young, Y. 1980: Enumeration of particle-bound and unattached respiring bacteria in the salt marsh environment. - Appl. Environ. Microbiol. 40: 156-160.

Heiskanen, A.-S. & Kononen, K. 1994: Sedimentation of vernal and late summer phytoplankton communities in the coastal Baltic Sea. - Arch. Hydrobiol. 131: 175-198.

Herndl, G.J. 1988: Ecology of amorphous aggregations (marine snow) in the Northern Adriatic Sea. II. Microbial density and activity in marine snow and its implication to overall pelagic processes. - Mar. Ecol. Prog. Ser. 48: 265-275.

Hoppe, H.-G. 1981: Blue-green algae agglomeration in surface water: a microbiotope of high bacterial activity. - Kieler Meeresforsch., Sonderh. 5: 291-303.

Hoppe, H.-G., Kim, S.J. & Gocke, K. 1988: Microbial decomposition in aquatic environments: combined process of extracellular enzyme activity and substrate uptake. - Appl. Environ. Microbiol. 54: 784-790.

Iriberri, J., Unanue, M., Barcina, I. & Egea, L. 1987: Seasonal variation in population density and heterotrophic activity of attached and free-living bacteria in coastal waters. - Appl. Environ. Microbiol. 53: 2308-2314.

Jackson, G. 1990: A model for the formation of marine algal flocs by physical coagulation processes. - Deep-Sea Res. 37: 1197-1211.

Jackson, G. 1994: Particle trajectories in a rotating cylinder: implications for aggregation incubations. - Deep-Sea Res. 41: 429-437.

Kaltenböck, E. & Herndl, G.J. 1992: Ecology of amorphous aggregations (marine snow) in the Northern Adriatic Sea. IV. Dissolved nutrients and the autotrophic community associated with marine snow. - Mar. Ecol. Prog. Ser. 87: 147-159.

Kankaanpää, H., Korhonen, M., Heiskanen, A.-M. & Suortti, A.-M. 1997: Seasonal sedimentationof organic matter and contaminants in the Gulf of Finland. - Boreal Env. Res. 2: 257-274.

Karner, M. & Herndl, G.J. 1992: Extracellular enzymatic activity and secondary production in free-living and marine-snow-associated bacteria. - Mar. Biol. 113: 341-347.

Kirchman, D. 1983: The production of bacteria attached to particles suspended in a freshwater pond. - Limnol. Oceanogr. 28: 858-872.

Kirchman, D. & Mitchell, R. 1982: Contribution of particle-bound bacteria to total microheterotrophic activity in five ponds and two marshes. - Appl. Environ. Microbiol. 43: 200-209.

Kiørboe, T., Lundsgaard, C., Olesen, M. & Hansen, J.L.S. 1994: Aggregation and sedimentation processes during a spring phytoplankton bloom: a field experiment to test coagulation theory. - J. Mar. Res. 52: 297-323.

Kuparinen, J., Leonardsson, K., Mattila, J. & Wikner, J. 1996: Food web structure and function in the Gulf of Bothnia, the Baltic Sea. - AMBIO Special report 8: 13-21.

Lampitt, R.S. , Wishner, K.F., Turley, C.M. & Angel, M.V. 1993: Marine snow studies in the Northeast Atlantic Ocean: distribution, composition and role as a food source for migrating plankton. - Mar. Biol. 116: 689-702.

Leppänen, J.-M. 1988: Cycling of organic matter during the vernal growth period in the open northern Baltic Proper. VI. Sinking of particulate matter. - Finnish Mar. Res. 255: 97-118.

Leppänen, J.-M. & Kononen, K. 1988: Cycling of organic matter during the vernal growth period in the open northern Baltic Proper. III. Phytoplankton composition and estimation of loss rates of phytoplankton production. - Finnish Mar. Res. 255: 37-54.

Logan, B.E. & Alldredge, A.L. 1989: Potential for increased nutrient uptake by flocculating diatoms. - Mar. Biol. 101: 443-450.

Marchant, H.J., Watanabe, K. & Kawachi, M. 1996: Marine snow in Antarctic coastal waters. - Proc. NIPR. Symp. Polar. Biol. 9: 75-83.

McCave, I.N. 1984: Size spectra and aggregation of suspended particles in the deep ocean. - Deep-Sea Res. 31: 329-352.

Michotey, V. & Bonin, P. 1997: Evidence for anaerobic bacterial processes in the water column: denitrifcation and dissimilatory nitrate ammonification in the northwestern Mediterranean Sea. - Mar. Ecol. Prog. Ser. 160: 47-56.

Müller-Niklas, G., Schuster, S., Kaltenböck, E. & Herndl, G.J. 1994: Organic content and bacterial metabolism in amorphous aggregations of the northern Adriatic Sea. Limnol. - Oceanogr. 39: 58-68.

Paerl, H.W. 1976: Spesific associations of the bluegreen algae *Anabaena* and *Aphanizomenon* with bacteria in freshwater blooms. - J. Phycol. 12: 432-435.

Paerl, H.W. 1985: Microzone formation: it's role in the enhancement of aquatic N_2 fixation. - Limnol. Oceanogr. 30: 1246-1252.

Paerl, H.W. & Prufert, L.E. 1987: Oxygen-poor microzones as potential sites of microbial N_2 fixation in nitrogen- depleted aerobic marine waters. - Appl. Environ. Microbiol. 53: 1078-1087.

Passow, U., Alldredge, A.L. & Logan, B.E. 1994: The role of particulate carbohydrate exudates in the flocculation of diatom blooms. - Deep-Sea Res. 41: 335-357.

Ploug, H., Kühl, M., Buchholz-Cleven, B. & Jørgensen, B.B. 1997: Anoxic aggregates - an ephemeral phenomenon in the pelagic environment? - Aquat. Microbiol. Ecol. 13: 285-294.

Riebesell, U. 1991a: Particle aggregation during a diatom bloom. I. Physical aspects. - Mar. Ecol. Prog. Ser. 69: 273-280.

Riebesell, U. 1991b: Particle aggregation during a diatom bloom. II. Biological aspects. - Mar. Ecol. Prog. Ser. 69: 281-291.

Robertson, L.A. & Kuenen, J.G. 1984: Aerobic denitrification: a controversy revived. - Arch. Microbiol. 139: 351-354.

Shanks, A.L. & Reeder, M.L. 1993: Reducing microzones and sulfide production in marine snow. - Mar. Ecol. Prog. Ser. 96: 43-47.

Shanks, A.L. & Trent, J.D. 1979: Marine snow: microscale nutrient patches. - Limnol. Oceanogr. 24: 850-854.

Silver, M.W., Shanks, A.L. & Trent, J.D. 1978: Marine snow: a microplankton habitat and source of small-scale patchiness in pelagic populations. - Science 201: 371-373.

Simon, M., Alldredge, A.L. & Azam, F. 1990: Bacterial carbon dynamics on marine snow. - Mar. Ecol. Prog. Ser. 65: 205-211.

Smetacek, V.S. 1985: Role of sinking in diatom life-history cycles: ecological, evolutionary and geological significance. - Mar. Biol. 84: 239-251.

Smith, D.C., Simon, M., Alldredge, A.L. & Azam, F. 1992: Intense hydrolytic enzyme activity on marine aggregates and implications for rapid particle dissolution. - Nature 359: 139-142.

Stanier, R.Y., Doudoroff, M. & Adelberg, E.A. 1971: General microbiology. - The Macmillan Press Ltd, London, U.K. pp. 694 - 698.

Suzuki, N. & Kato, K. 1953: Studies on suspended materials. Marine snow in the sea. I. Sources of marine snow. - Bulletin of the Faculty of Fisheries of Hokkaido University, 4, 132-135.

Taylor, G.T., Karl, D.M. & Pace, M.L. 1986: Impact of bacteria and zooflagellates on the composition of sinking particles: an *in situ* experiment. - Mar. Ecol. Prog. Ser. 29: 141-155.

Turley, C.M. 1992: Formation, vertical flux and remineralisation of aggregates in the ocean: a short review. - Arch. Hydrobiol. Beih. Ergebn. Limnol. 37: 155-163.

van de Graaf, A.A., Mulder, A., de Bruijn, P., Jetten, M.S.M., Robertson, L.A. & Kuenen, J.G. 1995: Anaerobic oxidation of ammonia is a biologically mediated process. - Appl. Environ. Microbiol. 61: 1246-1251.

Vandevivere, P. & Kirchman, D.L. 1993: Attachment stimulates exopolysaccharide synthesis by a bacterium. - Appl. Environ. Microbiol. 59: 3280-3286.

Weiss, P., Schweitzer, B., Amann, R. & Simon, M. 1996: Identification *in situ* and dynamics of bacteria on limnetic organic aggregates (lake snow). - Appl. Environ. Microbiol. 62: 1998-2005.

Worm, J. & Søndergaard, M. 1998: Dynamics of heterotrophic bacteria attached to *Microcystis* ssp. (Cyanobacteria). - Aquat. Microb. Ecol. 14: 19-28.

Zimmermann, H. & Kausch, H. 1996: Microaggregates in the Elbe Estuary: structure and colonisation during spring. - Advanc. Limnol. 48: 85-92.

Zimmermann, H. 1997: The microbial community on aggregates in the Elbe Estuary, Germany. - Aquat. Microb. Ecol. 13: 37-46.

No. 37

A THEORETICAL AND EXPERIMENTAL STUDY OF THE SELF-SIMILARITY CONCEPT

A ONE-DIMENSIONAL THERMODYNAMIC AIR-ICE-WATER MODEL: TECHNICAL AND ALGORITHM DESCRIPTION REPORT

LITERATURE REVIEW ON MICROBIOLOGY OF AGGREGATES ORIGINATING FROM PHYTOPLANKTON BLOOMS

Merentutkimuslaitos
Lyypekinkuja 3 A
PL 33
00931 Helsinki

Havsforskningsinstitutet
PB 33
00931 Helsingfors

Finnish Institute of Marine Research
P.O. Box 33
FIN-00931 Helsinki, Finland

ISSN 1238-5328